Winter 2018

A Scientific Approach to Understanding the Head Trauma Endured by a Mixed Martial Arts Fighter

John William Michael Sorbello
Old Dominion University

A SCIENTIFIC APPROACH TO UNDERSTANDING THE HEAD TRAUMA ENDURED BY A MIXED MARTIAL ARTS FIGHTER

by

John William Michael Sorbello
B.S.M.E. December 2007, Old Dominion University

A Thesis Submitted to the Faculty of
Old Dominion University in Fulfillment of the
Requirements for the Degree of

MASTER OF SCIENCE

MECHANICAL ENGINEERING

OLD DOMINION UNIVERSITY
December 2018

Approved by:

Miltiadis Kotinis (Director)

Sebastian Bawab (Member)

Gene Hou (Member)

ABSTRACT

A SCIENTIFIC APPROACH TO UNDERSTANDING THE HEAD TRAUMA ENDURED BY A MIXED MARTIAL ARTS FIGHTER

John William Michael Sorbello
Old Dominion University, 2018
Director: Dr. Miltiadis Kotinis

The purpose of this research is to gain some insight on the type of head trauma an athlete may encounter during mixed martial arts (MMA) competition. These athletes endure continuous blows to the head throughout their training and fighting career. The knowledge obtained from this research may assist MMA athletes and trainers in assessing the way they train, how they compete and, more importantly, how long they choose to compete in their amateur or professional MMA career.

The analysis is performed by first creating a three-dimensional solid model of the human head based on geometric coordinates originally obtained from a cadaver. The geometry is then imported into a Finite Element Analysis (FEA) software and validated by simulating a benchmark model based on experimental results.

This research utilizes experimental data provided by the *National Geographic* on impact loads of various MMA striking techniques applied to the already validated geometry and FEA model to obtain the resulting pressure that occurs in the brain of the human head. These results are subsequently analyzed to determine how severe this trauma may be to an athlete. Key points such as ways to further improve the FEA results are also discussed.

This thesis is dedicated to Joe Sorbello and Susan Sorbello, my parents, and Melissa Sorbello, my wife, for helping me to become the person I am today. I love you all and will be forever grateful to you and for you, as you have all helped me open doors that I never once thought were obtainable. All three of these people have made such a huge impact in my life and have played a huge part in my success of meeting these educational goals. This thesis represents the conclusion of a major milestone in my education and a building block in my career as an engineer. The encouragement of my parents always allowed me to see college as a realistic goal. They guided me in that direction and even though I enrolled in college, it was difficult to visualize myself completing a degree. They kept me on track and even though I was derailed a couple of times, they always helped me find my way back. Their confidence and belief in me kept me moving forward until I realized my potential. Not only was I accepted into Old Dominion University's Bachelor of Science in Mechanical Engineering, but I also ended up graduating in good standing with a grade point average that exceeded Old Dominion University's requirement for entry into their Master of Science in Mechanical Engineering program. If it wasn't for my parents' endless encouragement and support, I never would have discovered my full potential and reached these goals, that at one point in time, seemed unobtainable. This degree helped me earn my first job as an engineer only weeks after graduation. Years later, I would meet my future wife and decide to continue my education. I choose to return to Old Dominion University and pursue a Master of Science in Mechanical Engineering degree to help further my career as an engineer. I was accepted into the program but found out early on that it would be no easy task. This program was very demanding of my time and attention and difficult for me to juggle while working full time. With the support, patience and unselfishness of my loving wife, I was able to not only complete this program but to excel.

ACKNOWLEDGEMENTS

There are four specific people in addition to the committee members who have contributed to the successful completion of this thesis. Those four individuals are Dr. Miltiadis Kotinis, Dr. Sebastian Bawab, doctorate student Michael Polanco, and Huntington Ingalls Industries (HII) mechanical engineer Matt Davis. Dr. Kotinis is a former professor of mine at ODU, who has supported me from day one as my thesis advisor. With his guidance, I was able to complete my master's program with a thesis I can be proud of. Dr. Bawab offered me his support by providing access to specific FEA software with nonlinear capabilities that would have otherwise been extremely difficult to obtain. Mr. Polanco and Mr. Davis unselfishly made themselves available to assist me in learning how to utilize the non-linear capabilities of FEA software. Each of these individuals was a key part in my success and I wish to extend my deepest thanks and appreciation to each of them. I would like to especially thank my thesis advisor, Dr. Kotinis for his untiring efforts and support. Thank you so much for your patience and hours of guidance on my research.

NOMENCLATURE

a	Acceleration, Area, Parabola Variable
ATD	Anthropomorphic Test Device
B.C.	Before Christ
BEM	Boundary Element Method
CAD	Computer-aided Design
CAE	Complete Abaqus Environment
CEL	Coupled Eulerian-Lagrangian
CSF	Cerebrospinal Fluid
CT	Computed Tomography
E	Young's Modulus
f	Force Vector
F	Force
FEA	Finite Element Analysis
FEM	Finite Element Method
FDTD	Finite-Difference Time-Domain
$\bar{g}_i^P$	Modulus Ratio in the First Term in the Prony Series Expansion of the Shear Traction Relaxation Modulus
G	Shear Modulus
G_∞	Short-Time Shear Modulus
G_o	Long-Time Shear Modulus
h	Height, Horizontal Coordinate of Parabola Vertex
HIC	Head Injury Criterion
HII	Huntington Ingalls Industries

ICP	Intracranial Pressure
k	Vertical Coordinate of Parabola Vertex
$\bar{k}_i^P$	Modulus Ratio in the First Term in the Prony Series Expansion of the Normal Traction Relaxation Modulus
K	Bulk Modulus, Stiffness
lb	Pound
l	Length
L	Length
m	Mass, Meter
mm	Millimeter
mmH_20	Millimeter of Water
mmHg	Millimeter of Mercury
ms	Millisecond
M	Mass
MMA	Mixed Martial Arts
MRI	Magnetic Resonance Imaging
N	Number of Terms, Newton
NFL	National Football League
ODU	Old Dominion University
Pa	Pascal
s	Second
SAS	Subarachnoid Space
t	Time
TBI	Traumatic Brain Injury

UFC	Ultimate Fighting Championship
VHP	Visible Human Project
x	Displacement Vector of x-axis, Horizontal Coordinate from Parabola Vertex
$\ddot{x}$	Acceleration Vector of x-axis
y	Displacement Vector of y-axis, Vertical Coordinate from Parabola Vertex
β	Decay Constant
ρ	Density
τ_1	Relaxation Time for the First Term in the Prony Series Expansion
θ	Angle
ν	Poisson's Ratio
ω	Natural Frequency

TABLE OF CONTENTS

Page

LIST OF TABLES

LIST OF FIGURES

Figure Page

CHAPTER 1

INTRODUCTION

In today's society, a person's safety is typically the primary focus in any job, no matter what industry they may work in. Even if that industry is sports entertainment, safety should be of the utmost importance. It's not uncommon to hear in the news that a National Football League (NFL) quarterback was sidelined in a game because of a concussion or a retired middle-aged, heavyweight boxer is experiencing early signs of dementia due to repeated head trauma. Due to these now common and frequently occurring reports, it is just as important for these athletes to understand the dangers of receiving trauma to the head as it is for an electrician to understand the dangers of working with a live current in a damp or wet environment.

One form of the sports entertainment industry that is receiving a lot of attention these days is professional and amateur combat sports. One combat sport that is quickly gaining global popularity is mixed martial arts, also referred to as MMA. The purpose of this research is to take a scientific approach into understanding the head trauma that an MMA fighter may endure in competition. The sport of MMA carries a high probability of injury, so it's important that these athletes have an understanding of their body's capabilities as well as its limits.

This research is accomplished by collecting experimental impact data resulting from experienced MMA fighters demonstrating specific types of strikes. The data is then applied to a three-dimensional discretized model of the human head. The results of this analysis provide insight on the potential stress and strain that these fighters may encounter during competition. By understanding what may occur will allow these athletes and their trainers to make better, informed decisions on how they train, how they compete, and even how long they plan to participate in this

type of lifestyle. The potential knowledge that can be obtained from this type of research can very well make a difference in an MMA fighter's quality of life both inside and outside of competition.

1.1 SAFETY REGULATIONS IN MIXED MARTIAL ARTS

Competition in combat sports can be dated as far back as 648 B.C., when the sporting event known as Pankration was introduced into the Greek Olympic Games (Georgiou, 2008). Athletes who participated in Pankration would use grappling, submission holds, kicking and striking, both while standing and on the ground. The goal of this competition was to submit your opponent with a choke hold or joint lock, i.e., choke your opponent into unconsciousness or knock them unconscious with a strike, which many times, resulted in death. The only enforceable rules were no biting and no gouging of the opponents' eyes.

Today, Pankration can be primarily compared to MMA fighting, which is a combination of various unarmed fighting techniques, practices and disciplines that have been developed around the globe such as boxing, wrestling, Muay Thai kickboxing, Brazilian Jiu-Jitsu, Karate, Taekwondo, and Judo.

Although, there are many more safety regulations (UFC, 2018) in today's MMA competition, long-term effects are still a serious concern.

1.2 COMMON INJURIES IN MIXED MARTIAL ARTS

In MMA competition, precautions are made to enhance a fighter's safety by enforcing four main types of safety equipment (Gleiber, 2018). The primary along the latter is that each fighter that competes in MMA must have their hands bandaged in soft gauze cloth with a length no longer than 15 yards and a width no longer than two inches. This cloth shall be evenly distributed across the hand and secured with surgeon's adhesive tape near the wrist. The goal is to provide support to the fighter's wrist and knuckles (UFC, 2018).

A second form of safety equipment is the gloves that these fighters must wear over their bandaged hands. These gloves are designed to add a little more protection to the fighter's hands. They are open-fingered gloves as to not interfere with a fighter's ability to grapple and typically weigh no less than 4 ounces and no more than 6 ounces.

A third form of safety equipment MMA athletes are required to use in competition is a mouth guard. Mouth guards are used to protect not only the teeth but the gums and lips as well. It is also believed by some that mouth guards have the potential to prevent or reduce the severity of concussions in the event of a jaw injury.

The fourth form is an athletic cup, also known as a groin protector. This type of equipment prevents trauma to the groin of male athletes, specifically blunt force to the testicles. This type of impact is not only known to cause extreme pain but sometimes even nausea, a decrease in heart rate, dizziness, high body temperature, and decreased blood flow that may even cause some to lose consciousness. Unfortunately, at this point in time, female MMA fighters are prohibited from wearing groin protectors.

Although the aforementioned equipment is designed to protect the fighters and increase the longevity of the fight, severe injury is still very likely to occur. It is important to keep in mind that MMA athletes wear very little protective equipment, which makes fractures of the shins, hands, arms, and orbital bones common, whether from strikes or submission attempts. Fractures are very common in MMA and, although these injuries can be treated, the recovery is often long term.

Hand wraps and gloves may reduce the likelihood of hand injuries, but they won't prevent them. With each strike made by the fighter's hands, the probability of the fighter jamming their fingers, tearing ligaments, and even breaking their fingers increases. These injuries may appear to be minor in comparison to other injuries, but they still have the potential to temporarily disable a fighter and prevent him or her from participating in future competition for a long period of time.

Joint injuries such as a twisted knee, dislocated shoulders, and/or hyperextended elbows can occur often, especially during submission attempts when the joint is forced into awkward positions. Although these injuries may at times appear to be superficial, they can actually be pretty severe, resulting in torn or severed ligaments, tendons, and tissue. A long recovery time is often required, and the odds of complete recovery are minimal. In most cases, surgery may be the fighter's best chance at achieving complete recovery.

The worst-case injury a fighter may endure is a concussion, which is also known as a traumatic brain injury (TBI). In layman's terms, concussions can be described as violently shaking the brain. These injuries can affect the brain function, manifesting in the form of headaches, diminished concentration, loss of balance and/or coordination, and even memory loss. Fighting while concussed or repeated head trauma after a fighter sustains a concussion could lead to permanent brain damage such as degenerative brain disease.

1.3 LITERATURE REVIEW

Various attempts to build an FEA model of the human head capable of simulating brain injury have been successfully performed by many subject matter experts. Specifically, researchers have attempted to develop an FEA model in order to validate their computational methods using the results of Nahum's experimental (Nahum et al., 1976) and computational research (Nahum et al., 1977). Nahum and his research group had the resources to perform experimental impact tests on un-embalmed human cadavers. One series of experiments consisted of individual experiments on different specimens, while the other consisted of a series of multiple impacts on a single specimen. In an effort to replicate a subset of those experiments, a number of technical papers were reviewed to gain a better understanding on how to build an FEA validation model. These papers are discussed in more detail below and were used throughout this research as a guide.

The paper by Baeck, Goffin, & Vander Sloten (2011) focuses primarily on the impact of the cerebrospinal fluid (CSF) on the FEA simulation results. The authors develop a total of twelve finite element mesh models with simplified geometry consisting of the skull, CSF, and brain that are comparable in size to that of a standard human head. The simplified geometry allowed the authors to achieve excellent mesh quality. A variety of parameters are tested using the FEA software LS-DYNA. The parametric investigation includes testing models with different number of element layers through the thickness of the CSF. Furthermore, the CSF is treated as an elastic material with varying bulk modulus and shear modulus values in some models and in others is treated as a fluid with varying bulk modulus values.

The article by Belingardi, Chiandussi, & Gaviglio (2007) discusses in detail a finite element model with a refined mesh that utilizes geometrical data from computerized tomography (CT) and magnetic resonance imaging (MRI) images. The bone and tissue models consist of compact bone, cancellous bone, facial bone, brain, CSF, ventricles, scalp, dura mater, tentorium, and falx. However, all the organs/tissue modeled are continua, meaning the adjacent elements between the mating parts are not discreet. Each tissue is modeled as linear elastic, including the CSF. The brain material, on the other hand, is modeled as viscoelastic. A pressure distribution is applied to the frontal region of the skull to simulate Nahum's impactor without actually modeling it. Due to the short, 15-ms duration of impact, the model is not constrained in either translation or rotation. The FEA software used to solve this model is LS-DYNA.

Ganpule (2013) in his Ph.D. thesis utilizes the geometry from detailed MRI images produced by the Visible Human Project (VHP), which is segmented into four different bone and tissue types. These types include the skin, skull, subarachnoid space (SAS) and the brain. The FEA solver/model used an advanced method of analysis called Euler-Lagrangian coupling, with the

skin, skull and SAS being Lagrangian and the brain Eulerian. The FEA software utilized to solve this model is Abaqus/CAE.

Sayed et al. (2008) use MRI scans to create a detailed solid model of the human head consisting of the skull, CSF, gray brain matter, white brain matter, the cerebellum, corpus callosum, telencephalic nuclei, brain stem, and ventricles. The brain material consists of elastoplastic and viscoelastic material properties. The load is applied without simulating the impactor but, instead, applying a pressure load over the frontal area of the skull. Instead of applying the load at a 45-degree angle as done by Nahum (1977), it is applied at a calculated 36.2-degree angle.

Horgan & Gilchrist (2003) concluded that the depth and volume of the CSF and the thickness of the skull play a significant role in building a validation model. The authors of this paper also utilize solid models constructed from CT and MRI scans, while assigning viscoelastic material properties to the brain. In order to successfully simulate Nahum's experiments, free constraints are used in addition to a reduced impact load.

Kang, Willinger, Diaw, & Chinn (1997) replicate Nahum's experimental results (1977) by modeling the skull as a three-layer shell to permit bone fracture and connect each bone/tissue by applying a continuous mesh. Unlike most other FEA models, that particular validation model incorporates the impactor in the simulation, which has free boundary conditions. The impactor is positioned at a 45-degree angle with a prescribed velocity profile.

1.4 THESIS LAYOUT

In this thesis, details of the anatomy of the human head, consisting primarily of the skull, CSF, and brain are provided in Chapter 2. The description of the human head anatomy is required in order to describe the development of the solid model in Chapter 3, in addition to the experimental data obtained by Nahum and the differences between the experimental and the

computational model. The theory behind the FEA pertaining to the software Abaqus/CAE is provided in detail in Chapter 4, followed by a detailed explanation of the validation model and the corresponding results in Chapter 5. Those details include a summary of the analysis attempts made using various modeling assumptions, the results computed from the selected validation FEA model, and an interpretation of those results. A summary of the MMA striking experiments performed by *National Geographic* is provided in Chapter 6, followed by a description of the necessary modifications made to the aforementioned validation model to create the individual MMA models. The FEA results obtained for each MMA model are also presented in Chapter 6, together with an interpretation of those results. Finally, a discussion of the quality of the results obtained through this research is provided in Chapter 7, in addition to potential modifications that may improve the accuracy of the results in future research.

CHAPTER 2

ANATOMY OF THE HUMAN HEAD

2.1 SCALP

The scalp covers the human head by stretching from the hairline at the back of the skull to the eyebrows. It's the first line of defense in protecting the head and consists of the following five different layers (Abrahams, 2007): the skin, the connective tissue, the epicranial aponeurosis, the loose areolar tissue, and the pericranium.

The skin contains hair and sebaceous glands, which are microscopic exocrine glands that secrete oils to lubricate the skin and hair. It is the outermost layer on the head and the first line of defense for the head. The connective tissue, also known as the superficial fascia, is the second most outer layer of the scalp that connects the skin to the epicranial aponeurosis. It's a dense layer of fat containing the nerves and vessels of the scalp.

The aponeurosis also known as the epicranial aponeurosis, or the galea aponeurotic, is the third most outer layer of the scalp. It's a tough layer of dense fibrous tissue that allows fluids and blood to pass from the scalp to the upper eyelids. The loose areolar tissue is the fourth most outer layer of the scalp that connects the aponeurosis to the pericranium but also allows the outer three layers (i.e. skin, connective tissue and aponeurosis) to move freely. Certain veins are allowed to traverse this layer.

The pericranium is the inner most layer of the scalp. It's a dense layer of vascular connective tissue covering the cranial bones at the surface. This layer not only provides nutrition to the bone but also the capacity for repair.

2.2 CRANIAL BONES

Cranial bones and, in general, all bones, structurally consist of a mixture of both organic and inorganic materials. In other words, bones are considered complex natural composite materials (Hashemi & Smith, 2006). The inorganic portion consists of a bone mineral known as hydroxyapatite, which gives a bone its hardness. The organic portion primarily consists of collagen, which gives a bone its flexibility. In addition to being a composite material, the mechanical behavior of a bone is considered to be anisotropic and viscoelastic. By being anisotropic, the bone's mechanical behavior changes depending on whether the load being applied is in the longitudinal or in the transverse direction. With bone being viscoelastic, it responds differently depending on the speed to which the load is applied and the length of time the load is applied.

The human skull consists of six different types of cranial bones that encase the brain such as the frontal, parietal, occipital, temporal, sphenoid and ethmoid bone (Lazo, 2015). The frontal bone, also known as the forehead or anterior roof of the skull, extends down from the coronal suture, which is an immovable joint, to the frontonasal suture to form the upper surfaces of the orbits (eye sockets). Two parietal bones exist and are separated by the sagittal suture, which is the suture that spans down the center of the skull from the coronal suture to the lambdoid suture. These two bones make up the posterior roof of the skull. The occipital bone is the rear-most portion of the cranium that attaches to the parietal bones at the lambdoid suture. This bone also surrounds the brainstem and cerebelli (i.e. posterior cranial fossa). The temporal bone exists on both sides of the cranium below the parietal bones and attaches at the squamous suture. These bones are located above and behind the ears. The sphenoid bone is located anterior to the temporal bones and forms the base of the cranium behind the orbitals. The ethmoid bone is located inferior to the frontal bone and anterior to the sphenoid bone.

All six types of cranial bone discussed above are also known as flat bones. Flat bones (Abrahams, 2007) consist of two outer thin layers of cortical bone (also known as compact bone) enclosing a third inner layer known as the cancellous bone (also known as the diploë bone). Compared to the cancellous bone, the cortical bone has a higher density and is stronger and stiffer (Hashemi & Smith, 2006). The cortical bone is made of structural units called osteons, which are elongated cylinders that lie parallel to the long axis of the bone (Abrahams, 2007). Each osteon consists of multiple hollow tubes known as lamellae that are arranged concentrically to one another with collagen fibers running adjacent on each lamellae but in opposite directions. Just as a bundle of sticks tied together is stronger when compared to each individual stick, this natural design of the osteon not only improves the cortical bone's strength but also its resistance to torsion.

As stated previously, the cancellous bone is much lighter and less dense then the compact bone due to the number of cavities present. The networks of bony supports, which form the meshwork of cavities, are known as trabeculae. The trabeculae give the cancellous bone its "spongy" description as well as its strength.

2.3 MENINGES

The meninges are a thick fibrous tissue that lines the inner layer of the skull and provides protection to the central nervous system. They consist of three layers that cover the brain and extend down to the spinal cord. The first and outermost layer is the dura mater, the middle layer is the arachnoid mater, and the innermost layer is the pia mater.

The dura mater is a loosely arranged, fibro elastic layer of cells consisting of two layers. The first and outermost layer of the dura mater is the endosteal layer and the innermost is the meningeal layer. Both layers are primarily bonded together with few areas being separate to form blood-filled cavities. The meningeal layer contains larger blood vessels that split into capillaries in the pia mater. It also consists of four folds in the cranial cavity, known as dural folds that help

restrict rotatory displacement of the brain. These folds are known as the falx cerebri, tentorium cerebelli, falx cerebelli and the diaphragm sellae.

The middle layer of the meninges, known as the arachnoid mater is a thin transparent membrane that follows the contours of the dura mater. The purpose of this layer is to cushion the central nervous system. The arachnoid mater connects to the pia mater by bands of web-like tissue called trabeculae.

The innermost layer, also known as the pia mater firmly adheres to the surface of the brain and spinal cord. This is also the mater that the blood vessels pierce to feed the brain and spinal cord. The space between the arachnoid mater and pia mater is filled with cerebrospinal fluid.

2.4 CEREBROSPINAL FLUID

Cerebrospinal fluid (CSF) is a clear, colorless fluid that the brain floats in within the skull. CSF is produced and transferred throughout the cranial cavity by ventricles within the brain. This fluid is renewed about four to five times a day and serves three primary functions. First off, it removes waste products associated with neuronal activity and provides nutrients to the brain. The second function of the CSF is to provide a cushion for the brain to protect it when it collides with the skull. Last but not least, the CSF serves a vital function in the cerebral autoregulation of cerebral blood flow.

2.5 BRAIN

The brain is the primary component in the human body that controls all vital and non-vital organs. The reaction of a person's five senses; sight, hearing, smell, tastes and touch begins with the brain interpreting information from the environment. When the body reacts to stress or stimulus, it automatically attempts to stabilize itself by adjusting its temperature, blood pressure, heart rate, breathing, etc. This could not be possible without the brain relaying signals to the necessary organs. It controls a person's balance when walking, standing, and sitting. When you

talk, think, dream, or experience any type of emotion, it all begins with the brain. With the assistance of the spinal cord and peripheral nerves, the brain is the headquarters for the central nervous system, which is the system that processes and controls information and regulates all the conscious and unconscious facets of a person's life.

Each of the six primary external sections of the brain plays a specific role in a person's mechanical, emotional, and cognitive well-being. The frontal lobe is responsible for motor control, problem solving, and speech production. The parietal lobe identifies touch perception, body orientation, and sensory discrimination. The temporal lobe is responsible for auditory processing, language comprehension, and memory retrieval. The occipital lobe controls sight, visual reception, and visual interpretation. The cerebellum is where balance and coordination are controlled. The brainstem is responsible for involuntary responses.

CHAPTER 3

DEVELOPMENT OF THE FEA MODEL

Prior to performing a finite element analysis on the potential head trauma endured by a human due to MMA strikes, an FEA model is developed and validated. This is accomplished by partially replicating the model used in Nahum's experiments (Nahum et al., 1976). Nahum performed head impact experiments on intact human cadavers and successfully replicated the pertaining results using FEA (Nahum et al. 1977). Those publications have been the baseline for many researchers involved in studying brain trauma due to head impact. The validation model created for this research is discussed in depth by first describing how the experimental data was obtained by Nahum. This is followed by a detailed description of the solid modeling and of the FEA process employed to successfully replicate Nahum's experimental results.

3.1 DESCRIPTION OF NAHUM'S EXPERIMENTAL METHOD

A brief summary of the experimental process utilized by Nahum and Smith (1976) to obtain the experimental data (Nahum et al., 1976) is provided in this section. The human cadavers used in those experiments, and described in Nahum and Smith (1976), were completely intact and not embalmed. Therefore, the head still contained cerebrospinal fluid, and the brain contained cerebral blood vessels. Hence, when preparing the specimens, the cadavers were stored in a refrigerator that maintained a temperature of 2°C and relative humidity of 68%. Prior to the experiment, the specimens were removed to anthropometric dimensions such as height, weight, and skull geometry. Acceleration transducers were attached to the skull and catheters inserted into the vascular and CSF compartments, both which will be described in further detail.

In order to mount the acceleration transducers, the soft tissue overlaying the euryons, the point on either parietal bone marking either end of the greatest transverse diameter of the skull,

was excised to expose the cranial bone. Surface irregularities on the euryons were then ground off using an end mill machine tool. Liquid ether was applied to the location of the skull where the accelerometer mounting blocks were located to remove surface moisture. The accelerometer mounting block pairs were then positioned and attached to these sites on the axis normal to the mid-sagittal (perpendicular to your chest) plane using a resin-catalyst epoxy cement.

With the internal organs not functioning, there was no cardiac cycle to maintain blood flow, blood pressure, or CSF pressure. Under those circumstances, the blood (and the CSF) only respond to gravitational forces, meaning that the blood will just pool, thus, mechanical intervention was required. To resolve the issue of blood flow and pressure, arterial catheters were inserted bilaterally through the neck and into the carotid and vertebral vessels. These vessels are what supply your head, brain and spinal cord with blood. The catheters were used to pump fluid, such as normal saline and India ink (i.e. tracer), as needed into the cerebral blood vessels to maintain a pressure of 148 mm-Hg. To maintain the CSF pressure, holes were drilled bilaterally in the superior aspect of the frontal bone. An 18-gauge needle was then introduced into the brain, directly into the right and left lateral ventricles where the CSF is produced. The needle was subsequently removed and replaced with a catheter to allow constant removal or addition of normal saline to as needed to maintain an average pressure of 74 mm-H_2O. Holes were then drilled behind the catheter entry points and the meninges were punctured to vent air introduced into the skull cavity during this process. Both of these processes were done with the goal to simulate in vivo pressure-volume characteristics of the cranial fluid compartments.

Prior to performing the experiment, the specimen was seated with its back secured to a rigid support to minimize movement of the upper torso. The head was rotated forward at a 45° angle from the Frankfort Plane. Sutures were attached to each ear, while the free end was secured to an overhead frame to aid in securing the skulls position. However, the skull was not restrained

against anterior (forward) – posterior (rear) movement. The impactor was projected laterally along the mid-sagittal plan, contacting the skull at a 45° angle on the frontal bone. Constant velocity of the impactor prior to impact was controlled using an elastic shock cord propelled carrier mass. The carrier mass was equipped with linear ball bushings. The impactor mass was coupled to the carrier mass by two rods that inserted into these bushings. The carrier mass was accelerated to a predetermined velocity and then arrested. Once the carrier mass was arrested, the bushings allowed to the impactor mass to continue traveling at the predetermined velocity, while restraining it laterally. To minimize the possibility of skull fracture, padding varying in density and thickness was applied to the contact surface of the impactor prior to each experiment.

Data was collected using a variety of methods. The severity of each blow was analyzed by taking biaxial acceleration measurements of the skull's impact response. Once sufficient time had passed after the experiment, an autopsy of the intracranial contents was performed. Trauma was evaluated during this autopsy by using India ink carbon dye as a tracer to locate sites of vessel hemorrhage. The brain was also examined for signs of damage such as rupturing of the surface vessels and India ink leaking. The brain was then removed for examination and sectioned to examine the deep tissue locations for India ink carbon dye.

3.2 SOLID MODELING ATTEMPTS

Multiple attempts were made as part of this research to create a validation model that replicated Nahum's results. With each attempt, the geometry of the solid model was fine-tuned and simplified. A series of attempts were made ranging from data supplied from NEVA Electromagnetics, to using FEMAP and Autodesk Inventor.

Nahum et al (1976) provides the basic dimensions (in millimeters) for the skull that were measured from the cadavers used in their experiments and in their computational analysis (Nahum et al, 1977). The specific experiment utilized for validation purposes is Experiment No. 37 (Nahum

et al., 1976). The thickness of the skull was obtained from (Abrahams, 2007), which lists the diploë (inner section) thickness as 3 mm and the compact (outer sections) thickness as 2 mm. This equates to a 7 mm thick skull. Furthermore, the data found in (Kang et al., 1997) was proven to be a valid source since the authors were able to successfully replicate Nahum's experimental results. Since Nahum only provided dimensional properties for the skull, the volume of the brain and of the CSF became largely dependent on the overall mass of the human head assembly. Per Kang et al. (1997), the mass of the standard human head assembly is approximately 4.7 kg. However, the impactor dimensions used in the preliminary part of this research were based on the 5.59 kg mass provided by Nahum (Nahum et al., 1977) in conjunction with the dimensions found in (Song et al., 2015).

3.2.1 NEVA Electromagnetics – Human Head Solid Modeling

NEVA Electromagnetics is a technology-focused firm that specializes in electromagnetic modeling, creation of digital human body models, and antenna design (NEVA Electromagnetics, LLC, 2017). This company is well known for its image segmentation and generation of computational human models, such as their Visible Human Project (VHP) led by Sergey Makarov at the Worcester Polytechnic Institute of Massachusetts. The data obtained from the VHP is accessible to the public and allows for accurate Finite Element and Boundary Element modeling, and also Finite-Difference Time-Domain (FDTD) modeling. In other words, this model makes it possible to perform experimental research that is not safe to perform on a live human test subject. For example, as described in (Makarov et al, 2015), a metal hip is incorporated into their model and studies the effects of putting it in a Magnetic resonance imaging (MRI) scanner. The MRI's strong magnetic field can heat up a metal implant, causing pain, discomfort, and/or damage to patients. This is a common problem in all medical facilities, but with the data obtained from the VHP, safer, more effective scanning procedures for people with implants may be implemented.

The geometry data obtained from NEVA Electromagnetics proved to be insufficient for this particular research. The three-grid triangular plate elements for each part formed a hollow model. To remedy this, the NEVA Electromagnetic data was reformatted to be compatible with the FEA software called FEMAP. The reformatted data was then imported into FEMAP, where the hollow interior of each part's walls could be meshed with ten-node, tetrahedral solid elements, as shown in Fig. 1. Once this was accomplished, the original plate elements were

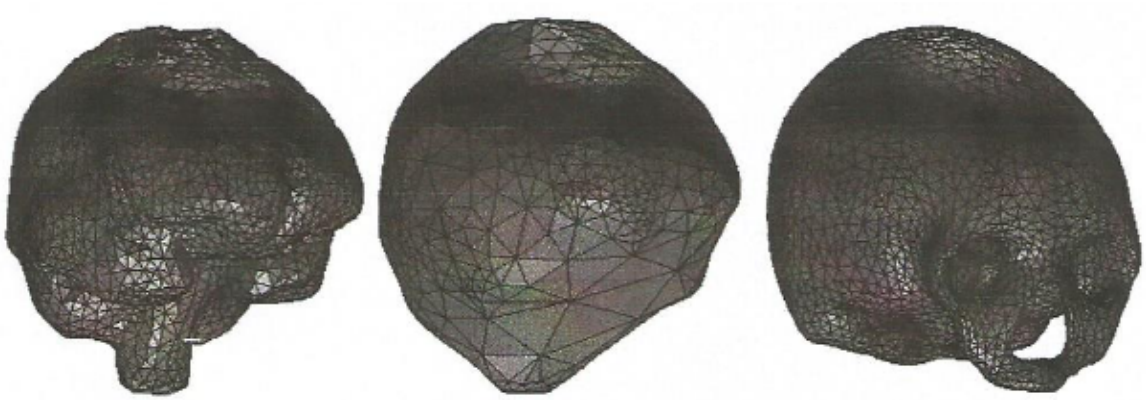

Figure 1: Human Head Solid Geometry (from left to right: brain, CSF, and skull)

deleted. The complexity of the resulting geometry only allowed tetrahedral elements. Most FEA programs with non-linear solver capabilities, including FEMAP, are known to produce poor results when tetrahedral elements are used, which was the case with this geometry.

3.2.2 Autodesk Inventor – Human Head Solid Modeling

Autodesk Inventor is a software with the capability of producing 2D drawings and 3D solid models. This software provides an array of file types that are compatible with most FEA programs, making it easy to import them directly into the chosen software. During the first attempt at creating 3D solid model parts, displayed in Fig. 2, an effort was made to model the brain with the frontal lobe, parietal lobe, occipital lobe, temporal lobe, cerebellum and brain stem.

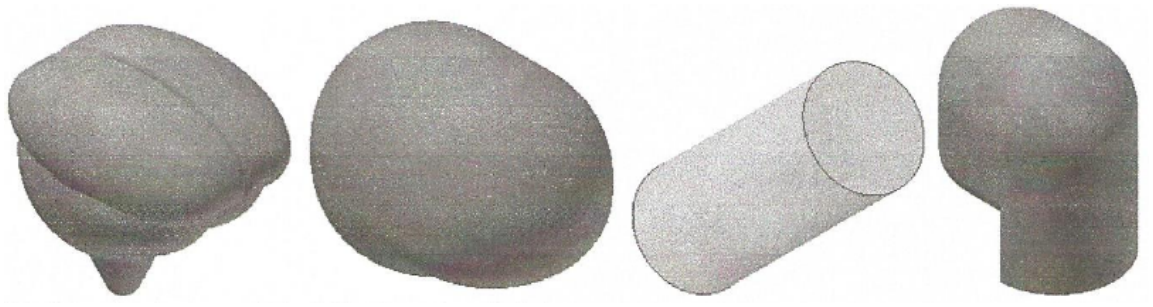

Figure 2: First Solid Modeling Attempt using Autodesk Inventor (from left to right: brain, skull, impactor, and skull)

An opening in the base of the skull and CSF was also incorporated for the brain stem to pass through. Each part was modeled to equate to a specific volume. These volumes were multiplied by densities based on data available in Willinger et al. (1999) to obtain the total head mass reported in Kang et al. (1997). It should be noted that in the latter article, the authors report results obtained using FEA that are very close to Nahum's experimental results (Nahum et al., 1977) in this solution attempt, a solid model of the impactor was also incorporated. Due to the complexity of the geometry, e.g. number of radii, the FEA software could not produce a 100% hexahedral mesh. Instead, it was primarily tetrahedral and, as discussed in Section 3.2.1, most FEA programs with non-linear solver capabilities produce poor results when tetrahedral elements are used. In addition, the thickness of the CSF was not consistent. Portions of it were abnormally thick and others extremely thin, which also became problematic when it came to element stability.

A second attempt, shown in Fig. 3, was made to produce 3D solid model parts using Autodesk Inventor, but this time it was decided to reduce the complexity of the geometry. For this purpose, the frontal, the parietal, the occipital, and the temporal lobe, and the cerebellum were merged. The brain stem was removed for simplicity. This caused the skull and CSF to be

completely hollow and encapsulate each other. The opening in the base of the skull and CSF was closed. In addition, the thickness of the CSF was modified to be consistent throughout.

Figure 3: Second Solid Modeling Attempt using Autodesk Inventor (from left to right: brain, CSF, skull, and impactor)

The model shown in Fig. 3 was imported in a different FEA software, Abaqus/CAE instead of FEMAP, but proved to be unsuccessful since 100% hexahedral elements was not achieved.

A third attempt was subsequently made to produce 3D solid model parts using Autodesk Inventor.

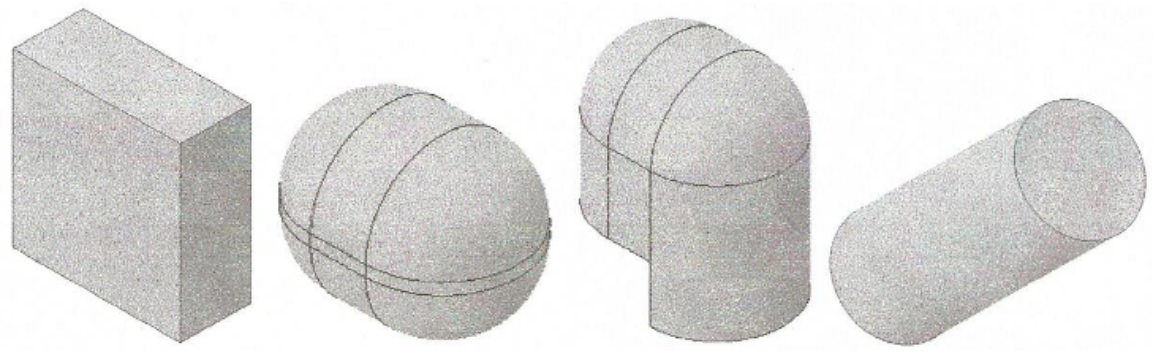

Figure 4: Third Solid Modeling Attempt using Autodesk Inventor (from left to right: computational domain / brain, CSF, skull, and impactor)

As shown in Fig. 4, the geometry was simplified even further by removing the cerebellum of the brain completely, as well as removing a few radii from the skull. This attempt proved to be successful at achieving a 100% hexahedral element mesh. As discussed previously, the modified geometry is developed in such a way that it maintains the desired volume to produce accurate weights. Furthermore, the brain was altered to encompass the entire model. This was done to support an alternate FEA solution approach, the coupled Eulerian-Lagrangian (CEL) solver, which is available in Abaqus/CAE. Subsequently, the brain volume was modeled to fit inside the CSF, as shown in Fig. 5, to allow for the utilization of the Lagrangian solver, which is available in Abaqus/CAE. This modification also proved to be successful in achieving a 100% hexahedral element mesh. The aforementioned solvers are discussed in detail in Section 4.5.

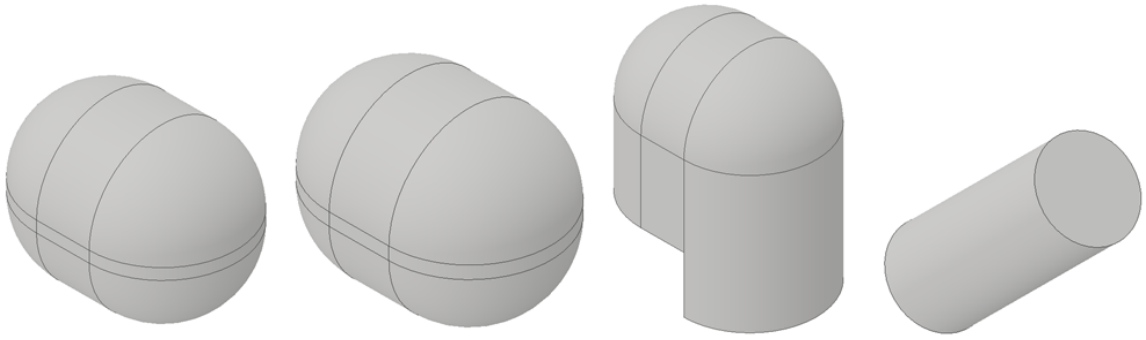

Figure 5: Modified Third Solid Modeling Attempt using Autodesk Inventor (from left to right: brain, CSF, skull, and impactor)

3.3 DETAILS OF THE SOLID MODEL GEOMETRY

The solid-model geometry was dimensioned in millimeters and modified in Autodesk Inventor by simplifying its geometry to obtain a 100% hexahedral mesh. Each part was imported in a .sat format as opposed to a .stp format because it was found that the .sat format is capable of supporting significantly more partitions with greater detail, which eventually led to obtaining a

100% hexahedral mesh. However, this modification proved to be risky due to the simplifications in the model geometry, but all critical dimensions remained intact. When each part was imported into Abaqus/CAE, it was scaled by a factor of 0.001 to convert all dimensions into meters.

The dimensioning of the skull remained consistent with Experiment 37, dimensions A - E displayed in Figure 10 in (Nahum et al., 1977). In addition, the skull maintained a minimum thickness of 7 mm. These dimensions and thickness led to a solid, hollow skull with an overall volume of $1.35 \cdot 10^6$ mm^3.

The dimensioning of the CSF was dependent on the inner skull cavity. It was given a consistent thickness of 2.125 mm. These dimensions equate to a volume of $0.161 \cdot 10^6$ mm^3 (162 mL). According to Lazo (2015), the total volume of cerebrospinal fluid in an adult human can range anywhere from 140 to 270 mL, but according to most expert sources, the average human head contains roughly 150 mL of CSF. The higher end of the volume range supported by the data in Lazo, 2015, improves the model's mesh by allowing two layers of thicker elements. Compared to the average 150 mL volume, this validation model contains 8% more cerebrospinal fluid, which is viewed as being acceptable.

The dimensioning of the brain was completely dependent upon meeting the dimensional constraints of the skull and the CSF. The total volume of the brain was calculated at $1.35 \cdot 10^6$ mm^3. These dimensions were verified by comparing the total mass of the combined skull, CSF and brain to the 4.70 kg mass of the human head used in (Kang et al., 1997).

The dimensioning of the impactor was based off the data in (Song et al., 2015), where an impactor with a total volume of $0.717 \cdot 10^6$ mm^3 is utilized. Multiplying this volume by the density of steel, i.e. 7,850 kg/m^3, equates to a 5.59 kg mass, which is consistent with the data for Experiment 37 in Nahum et al. (1977). These factors (i.e. mass and volume) led to the estimated

contact area of the impactor being 1,470 mm^2. Furthermore, the impactor's calculated surface area was key in defining the contact area nodes on the skull.

CHAPTER 4

FINITE ELEMENT ANALYSIS

Finite Element Analysis, also known as FEA, is a numerical approximation method for analyzing complex parts and assemblies under specified behaviors for an array of applications (i.e. solid, fluid, and/or thermal). Each part may be broken down into much smaller sections called elements by a process called meshing, with each element connected to one another by a node. Once this has been achieved, the section properties of the elements are defined. For example, elements may be classified as 2D line elements, 2D planar, or 3D solid. Then, material properties are assigned to each section property. Typical material properties include the density, the Young's modulus, and Poisson's ratio. To prevent the model from floating in space, boundary conditions must be applied. This can be done by constraining specified degrees of freedom (DOF) of specific nodes. Before solving the model, a load must be applied to the part or assembly. These loads are typically concentrated loads or bending moments, but they can also be prescribed accelerations, velocities, temperatures, etc. The FEA software then calculates an approximate solution for the unknown displacement. For example, to calculate the displacement of a solid body, the FEA software may use the stiffness (displacement) method, in which case, the vector of applied forces, $\{F\}$ is known:

$$\{F\} = [K]\{U\} \rightarrow \{U\} = [K]^{-1}\{F\}$$

The elements of the stiffness matrix $[K]$ are calculated based on material properties and geometry and, thus, are known. The above matrix equation is then be solved for the unknown displacements $\{U\}$ in each domain, i.e., group of elements. The methods used to calculate these the solution can be separated into two categories known as implicit and explicit time integration methods.

4.1 ELEMENT QUALITY

An FEA model relies heavily on the quality of its mesh. A mesh containing poor quality elements may result in multiple warnings or errors stemming from severe distortion while under load. To prevent quality issues from forming, there are some basic criteria that should be reviewed from the engineer that is building the FEA model. These criteria are the element aspect ratio, taper, skew angle, warping, and Jacobian ratio. Most FEA software comes with a built-in quality check with this specific criterion as a minimum.

The aspect ratio of an element is the ratio of its longest edge length to the shortest edge length. The ratio can be calculated by dividing the longest edge length by the shortest edge length. A ratio of 1:1 is ideal, but any ratio up to 10:1 is typically acceptable. Taper occurs in quadrilateral elements. FEA will check for the amount of deviation in the element from a rectangular shape. The ideal taper value would be 1, meaning it has a perfect rectangular shape with four 90-degree angles. An acceptable taper value would be between 0.5 and 1.

For tri-elements, a skew angle can be found by first drawing a line through the midpoints of two opposing sides that are connected by a common node. Then a second line is drawn from that common node to the midpoint of the adjacent side. The minimum angle created when the two drawn lines intersect and is subtracted from 90 degrees to calculate the skew angle. For a quad-element, two lines are drawn. Both drawn lines span between two opposing midpoints. The minimum angle is then subtracted from 90 degrees to calculate the skew angle. An acceptable skew angle is typically no more than 30 degrees.

Warping is the deviation from the best-fit plane that contains the element (Check Quality, 2012). Warping is calculated by splitting a quad element into two triangular sections and finding the angle between the two planes. The same procedure is performed using the opposite corners. The maximum angle found between the planes is the warping angle of the element. Ideally, the

value of the warping angle should be less than 20 degrees. The Jacobian ratio is the ratio of an ideal shaped element's determinate compared to the determinate of the deviated shape. Ideally, the Jacobian ratio would be as close to 1:1 as possible.

4.2 CONTACT MODELING

Contact in FEA is when two parts are constrained in such a way that when their surfaces touch, forces are transmitted from one part to the other. When the two parts are separated, no forces are transmitted. Most FEA software contains code that initiates a contact algorithm. The majority of these algorithms are general in nature and simulate the following Abaqus/CAE contact algorithm (Fig. 6) below. To perform this algorithm, the software must be capable of detecting when two surfaces are in contact in order to apply the proper constraints. When contact is initiated in FEA, each surface is defined as a slave or a master. Simply put, the deflection of the slave surface is dependent on the master surface. The slave surface is typically assigned to the smaller of the two parts or the part made of the softer material. Parts with slave surfaces are typically assigned a finer mesh and may be less stiff in comparison to the mating part. For example, if a model was created to simulate a hammer striking a nail, the contact region of the hammer would be classified as the master surface, while the head of the nail would be classified as the slave surface. The interaction between the master and slave surfaces of parts can be defined as either behavior normal to the surfaces or behavior tangential to the surfaces.

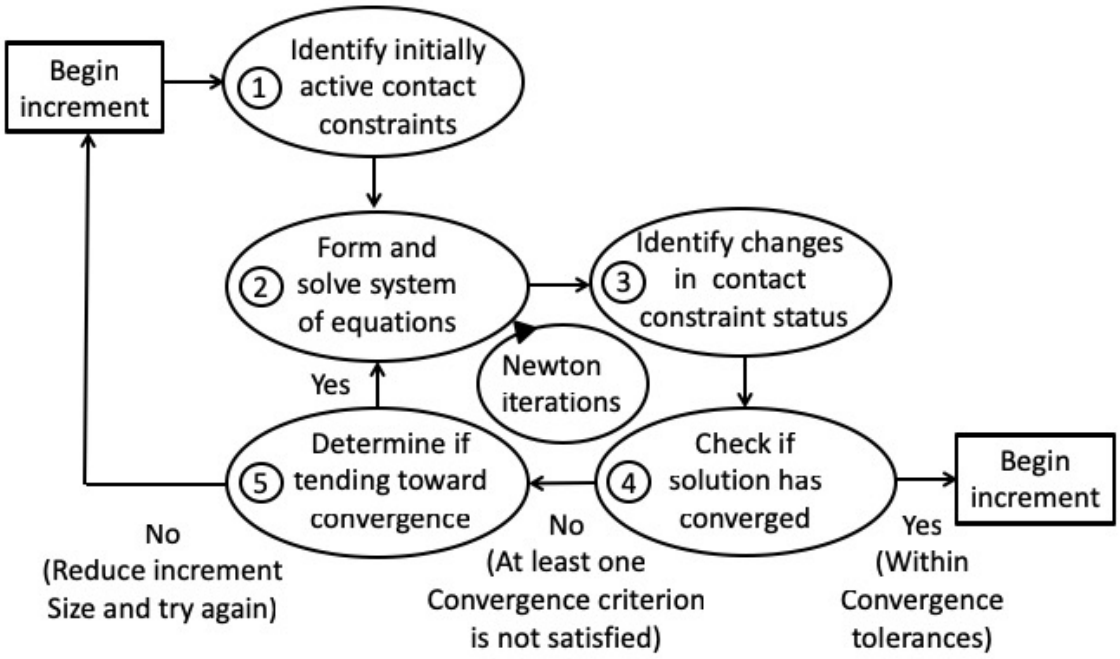

Figure 6: Abaqus/CAE Contact Modeling Algorithm

When contact occurs normal to a part's surface, the initial condition is typically a positive gap between the two contact surfaces. Once that positive gap between the surfaces becomes zero, the contact constraint is applied, and load is transmitted between the surfaces. Once that load becomes zero again, the contact constraint is removed, and a positive gap returns. This type of behavior is commonly known as "Hard Contact" in Abaqus/CAE.

Behavior tangential to the surfaces, mean non-normal contact forces are applied to the surfaces in question. When this type of behavior occurs, the contacting surfaces may encounter friction and/or sliding (i.e. no friction). When sliding occurs, careful consideration should be taken in regard to the model's boundary conditions, to avoid geometry flying into space, so to speak. When friction is applied, careful consideration should be taken regarding what friction coefficient to avoid reactions due to "sticking". When the contact forces produced may be a combination of both normal and shear stresses.

When utilizing contact interaction in FEA, it is very important to avoid surface-to-surface penetrations and node to surface penetrations. This can be controlled by invoking the constraint enforcement method, the contact surface weighting, or tie constraints.

The constraint enforcement method enforces contact constraints using what Abaqus/CAE refers to as the penalty contact method. This method allows the software to search for node, face and edge penetrations. When this search is complete, the software will apply a penalty stiffness factor to the slave and master's material that causes a contact force that is proportional to the penetration depth. This contact force is applied direction to the penetrating slave node and the reaction-distributed force is distributed between the master segment nodes (Jacob & Goulding, 2002).

Contact surface weighting only resists slave nodes penetrating into master facets (Getting Started with Abaqus: Interactive Edition (6.14), 2014). By invoking this method, the master-slave contact can become more balanced. Tie constraints prevent surface that are initially in contact from penetrating, separating and/or sliding. This is done by the software automatically fixing the slave nodes to the master surfaces. These constraints are particularly useful when dealing with significantly different mesh densities.

4.3 IMPLICIT TIME INTEGRATION

Implicit code operations fall under the steady-state or quasi-static category. These models are typically static or low velocity in nature such airflow over a wing, gravity load of a structure or simply solving model matrices (i.e. $\sum F = 0$). An implicit calculation begins with Newton's Second Law (Jacob & Goulding, 2002):

$$[M]\{\ddot{x}\} + [K]\{x\} = \{f_{ex}\}$$

This equation consists of a system mass matrix, $[M]$, stiffness matrix, $[K]$, nodal accelerations vector, $\{\ddot{x}\}$, nodal displacement vectors, $\{x\}$, and external force vectors, $\{f_{ex}\}$. Implicit time

integration focuses on displacement by inversion of the stiffness matrix, which may require an extensive amount of computer memory. Newton's Second Law is solved repeatedly at an initial step, *n* to step, *n+1* at variable time increments. After each time step is solved, equilibrium between the internal and external forces must be achieved. When this is achieved, average accelerations and displacements are calculated until convergence is reached. It's important to note that the displacements calculated in step *n+1* are a function of accelerations and displacements of step *n* (The Finite Element Method - Theory, 2017). Variable time increments may be used but if the solution is having difficulty reaching convergence, the time step may become very small resulting in the problem not converging at all. For this reason, it is strongly recommended not to use an implicit solver when tackling highly nonlinear problems. If the solution does converge, it can be very accurate.

4.4 EXPLICIT TIME INTEGRATION

Explicit code operations fall under the dynamic response category. These models are typically high velocity or short time events such as an explosion, chaotic flow, ballistic events, or high impact (i.e. $\sum F = ma$). Just as the implicit calculation, the explicit calculation also begins with Newton's 2nd Law (Jacob & Goulding, 2002):

$$[M]\{\ddot{x}\} = \{f_{ex}\} - [K]\{x\} = \{f_{ex}\} - \{f_{in}\}$$

This equation substitutes the stiffness force as an internal nodal force vector, $\{f_{in}\}$. Explicit time integration focuses on acceleration by inversion of the mass matrix. Typically, the masses are lumped together, and the mass matrix becomes a diagonal matrix, which greatly reduces the size of the matrices. From this point, the FEA program explicitly advances time to calculate the velocity and then displacement. Next, strains, stresses, and internal forces are calculated, followed by the calculation of a new time step. It's important that the time steps chosen, when using an explicit

solver, are smaller than the critical time step, which is dependent on the smallest element and the speed of sound in that material. The external forces are then evaluated and the process repeats.

4.5 EULERIAN AND LAGRANGIAN SOLUTION METHODS

The Eulerian solution method can be explained by observing the properties of a material over time and space. For example, a state trooper sets up a speed trap on the highway, but the radar gun only has a 500-foot range. That state trooper is limited to only recording the speed of drivers passing through while they are in that 500-foot window. In this example, the Eulerian mesh would be the 500-foot window, while the vehicles are the bodies that flow through it. The nodes of the Eulerian mesh remain fixed, while the material points move through the mesh.

The Lagrangian solution method can be explained as a particle being followed at each point, with the properties of that particle being determined as the particle moves. For example, a state trooper is passed by a driver that appears to be exceeding the speed limit. The state trooper then proceeds to pace the faulty driver to determine the driver's speed. In other words, the state trooper is tracking the object to determine its properties. In this example, the Lagrangian mesh would be drawn on the faulty driver's vehicle and the mesh would deform with the body (i.e. vehicle). Unlike the Eulerian mesh, both the nodes and material points of the Lagrangian mesh change position as the body deforms. However, the position of the material points relative to the modes remain fixed.

4.6 FINITE ELEMENT MESH

Each of the head parts was meshed independently and each part had to be partitioned into easily manageable sections. This was done to improve the mesh quality and the use of hexahedral elements as opposed to tetrahedral elements.

The brain, CSF, and impactor were all meshed with a structured technique, meaning the mesh was generated with a predefined topology primarily due to the symmetry in these parts. This

technique is ideal for creating square or cube elements out of the regions defined by the topology with the best quality achievable. The skull on the other hand was meshed with a mix of two techniques; the first being a structured technique, as discussed above, and the second one being a sweep technique. When the sweep technique is used, a region must be selected, and Abaqus/CAE then creates a mesh on one side of that region. This starting point is known as the source side. The software follows an edge or a sweep path as it builds the mesh to the final side known as the target side. The sweep technique is capable of creating a good quality mesh but not as great in comparison to the structured technique.

Each part was built with an explicit element mesh with a family classification. The family classification simply assigns the type of analysis that will be performed on the model. The CSF, brain, and skull were classified as a 3D stress family. For simplification, each part was assigned a linear geometric order of elements opposed to a quadratic, meaning that no mid-side nodes were assigned to the elements.

Each part was meshed with a specific seed (node) size that no only allowed the model to converge but also to obtain the best quality possible. The seed size for each part is listed in Table 1, along with each part's resulting node and element quantities.

Part	Seed Size (m)	# of Nodes	# of Elements
Brain	0.0030	97,764	93,136
CSF	0.0030	27,924	18,612
Skull	0.0070	9,030	5,404

Table 1: Validation Model Mesh Data

CHAPTER 5

VALIDATION MODEL ANALYSIS AND RESULTS

Multiple attempts were made to develop an FEA model that successfully replicated Nahum's experimental data. In the end, Abaqus/CAE proved to be the ideal program to build a non-linear FEA model that incorporated both elastic and viscoelastic materials. Before utilizing Abaqus/CAE, multiple attempts were made with MSC Nastran, LS-Dyna, and FEMAP. All three programs are widely used within the engineering disciplines and with the correct understanding of each program's capabilities; there are not many problems these programs cannot solve.

Abaqus/CAE is a software package used for both modeling and finite element analysis of individual parts and assemblies. This software allows the user to import models from compatible CAD software, in addition to having its own modeling capabilities. Not only does it perform finite element analysis with optional monitoring, it also performs post-processing. Abaqus/CAE supports linear, non-linear, and contact problems utilizing both implicit and explicit integration solution methods.

5.1 EQUATIONS OF MOTION

Abaqus/CAE performs its analysis using elemental time steps. This means that the user-defined solve time or time period, is broken up into steps, with each step assigned a time scale. The process used to calculate the elemental time steps is as follows:

Start with Newton's 2nd Law:

$$[M]\{\ddot{x}\} + [K]\{x\} = 0$$

Express Newton's 2nd Law in matrix format:

$$\frac{\rho AL}{2}\begin{bmatrix}1 & 0\\ 0 & 1\end{bmatrix}\begin{Bmatrix}\ddot{x}_1\\ \ddot{x}_2\end{Bmatrix} + \frac{EA}{L}\begin{bmatrix}1 & -1\\ -1 & 1\end{bmatrix}\begin{Bmatrix}x_1\\ x_2\end{Bmatrix} = 0$$

Express Newton's 2nd Law in eigenvalue format:

$$\frac{EA}{L}\begin{bmatrix}1 & -1\\ -1 & 1\end{bmatrix} - \omega^2\frac{\rho AL}{2}\begin{bmatrix}1 & 0\\ 0 & 1\end{bmatrix}\begin{Bmatrix}x_1\\ x_2\end{Bmatrix} = 0$$

The limiting value of ω^2 is obtained:

$$\begin{bmatrix}\left(\frac{EA}{L} - \omega^2\frac{\rho AL}{2}\right) & -\frac{EA}{L}\\ -\frac{EA}{L} & \left(\frac{EA}{L} - \omega^2\frac{\rho AL}{2}\right)\end{bmatrix} = 0$$

Evaluating the above determinant:

$$\frac{2}{\omega} = \frac{L}{\sqrt{E/\rho}} = \frac{L}{c} = \Delta t$$

The equation for calculating the elemental time step typically produces an accurate value. With this being the case, it is important to prevent the minimum time step value from approaching the specified maximum time step value (i.e. limit of stability). To assure the minimum limit does not approach the maximum limit, most FEA programs incorporate a scale factor. For the validation model, the time period is 7 ms, with a scale factor of 1.

5.2 MATERIALS

Each part is assigned a specific section type and material. The Lagrangian-mesh parts, i.e. CSF, brain, and skull, are each assigned to a deformable, solid, homogeneous type section. Each part's section also defines the material, thus, causing each section to be independent.

In order to determine the appropriate material properties for the FEA validation model, it was decided to start with the CSF, as the CSF is the part that dampens the brain motion upon impact. As is shown in Baeck et al. (2011), modeling the CSF material as a fluid could have a significant impact on the FEA results due to the potential large deformation of CSF elements. It is also shown that the lower the bulk modulus, for both the elastic and fluid models, the more unstable the model becomes. This results in a model displaying nearly incompressible behavior. That

research concluded that modeling the CSF material as elastic is ideal, since the fluid material is unstable in comparison.

The brain material simulated in the validation FEA model was assigned material properties combined from Baeck et al. (2011) and from Ganpule2013). Ganpule, obtained the three-dimensional geometry data from the Visible Human Project and utilized the coupled Eulerian-Lagrangian method. Although, the validation model created for this research utilizes the Lagrangian method, it was decided to experiment with the viscoelastic material properties from (Ganpule, 2013) due to Ganpule's success in simulating Nahum's frontal cadaveric impact experiment results. The remaining elastic properties were obtained from Baeck et al. (2011). The Poisson's ratio is kept constant at 0.49, but Young's modulus was decreased over time.

The brain for the validation model solved in this research was built with elastic, isotropic properties as well as viscoelastic. The time dependent shear modulus formula is used as illustrated below to obtain the corresponding Young's modulus and Poisson's ratio values.

$$G(t_0) = G_\infty + (G_0 - G_\infty)e^{-\beta t_0}$$

$$E(t_0) = \frac{9KG(t_0)}{3K + G(t_0)}$$

$$\nu(t_o) = \frac{3k - 2G(t_0)}{2[3K + G(t_0)]}$$

The viscoelastic properties were calculated using a time-domain Prony-series method. The Prony-series method was developed by Gaspard Riche de Prony in 1795 as a way of extracting material information from a one-dimensional relaxation test (Carriere & Moses, 1992). The Prony series for the shear and bulk relaxation is calculated as follows:

$$G(t) = G_\infty + \sum_{i=1}^{N} \bar{g}_i^P \, e^{-t/\tau_i}$$

$$K(t) = K_\infty + \sum_{i=1}^{N} \bar{k}_i^P \, e^{-t/\tau_i}$$

A correlation was found between the researched, time-dependent shear modulus equation and the Abaqus/CAE Prony Series equations. A MATLAB script was developed to calculate and optimize the Prony coefficients (i.e. $\bar{g}_i^P$, k_i^P, and τ_i) per the code outlined in Appendix A. The MATLAB script was built using three functions. The first function is title, *PronyC*, which applies summation constraints to the desired coefficients. When utilizing the Prony Series Method, the summation of the ratios must not exceed a value of 1.0. The second function, *PronyF*, calculates the prony shear modulus ratio $[g_P = G(t)/G_o]$ with the output coefficients and then calculates the error between this equation and the normal shear modulus ratio. The third function, *PronyOpt*, calculates the normal shear modulus and the normal shear modulus ratio $[g_n = G(t)/G_o]$. It then initiates the fuctions *PronyC* and *PronyF* to optimize the value of the prony shear modulus coefficients with a user-defined number of Prony coefficients (NPC=2) and equations (NTSP=250). MATLAB then outputs multiple potential values based for the modulus ratio in the Prony series expansion of the shear traction relaxation modulus, $\bar{g}_i^P$ and the relaxation time for the Prony series expansion, τ_i. This particular code calculated the modulus ratio in the Prony series expansion of the shear traction relaxation modulus ($\bar{g}_i^P$) as $\bar{g}_1^P = 0.8098$. Since the bulk modulus was not a time dependent factor within (Baeck et al., 2011) it was assumed not to be while utilizing the Prony Series Method as well. Therefore, the bulk modulus ratio in the Prony series expansion of the normal traction relaxation modulus ($\bar{k}_i^P$) is equal to $\bar{k}_1^P = 0.0$. The value for the relaxation time for the Prony series expansion (τ_i) is $\tau_1 = 0.0014$.

The skull for the validation model solved in this research was built with elastic, isotropic properties. The bone material properties assigned for the skull were common values used for cortical bone, also known as compact bone.

5.3 PRELIMINARY SOLUTION ATTEMPTS

The first solution attempt was performed by first importing the solid geometry shown in Fig. 3 (Section 3.2.2) into Abaqus/CAE in the .stp file format. However, a 100% hexahedral mesh could not be obtained. It was assumed initially that this would be the best course of action in achieving ideal quality elements. Although the majority of the model consisted of hexahedral elements, tetrahedral elements were still present within each part of the assembly.

Table 2 contains the material properties applied to each part. Furthermore, tie constraints were applied between the outer surface of the brain and the inner surface of the CSF, and between the outer surface of the CSF and the inner surface of the skull. The idea was to connect the mating parts to prevent penetration, as described in Section 4.2. This method was chosen in order to avoid creating elements that could potentially collapse on one another during impact loading. However, general contact properties were applied between the impactor and the skull. Fixed boundary conditions were applied to 45 nodes around the perimeter of the skull's base surface to prevent the skull from moving freely into space at impact. A constant velocity of 9.94 m/s (Nahum et al., 1977) was also applied as a boundary condition to the impactor's geometry.

The first attempt to solve an FEA model in Abaqus/CAE to validate Nahum's results was performed using an explicit solver and a Lagrangian approach. Unfortunately, that attempt proved to be unsuccessful. When solving the model, it was found that the ratio of deformation speed to wave speed exceeds 1.00 in multiple skull, CSF, and brain elements.

The second solution attempt was performed using an explicit solver and a coupled Eulerian-Lagrangian approach, and also the geometry illustrated in Fig. 4. Table 3 contains the updated material properties applied to each part.

Part	Type	Material Properties	Reference
Skull	Lagrangian	$\rho = 1{,}800\ kg/m^3$	(Kang et al., 1997)
		$E = 15.0\ GPa$	
		$\nu = 0.22$	
Brain	Lagrangian	$\rho = 1{,}140\ kg/m^3$	(Song et al., 2015)
		$K = 1.125\ GPa$	(Kang et al., 1997)
		$G_o = 49.0\ kPa$	
		$G_\infty = 16.7\ kPa$	
		$\beta = 0.000145\ s^{-1}$	
		$E = 146{,}998\ Pa$	Calculated
		$\nu = 0.48$	
		$\bar{g}_i^P = 0.8\ ,\ 0.0$	
		$\bar{k}_i^P = 0.0\ ,\ 0.0$	
		$\tau_i = 0.0125\ ,\ 0.2054$	
CSF	Lagrangian	$\rho = 1{,}040\ kg/m^3$	(Kang et al., 1997)
		$E = 12.0\ kPa$	Calculated
		$\nu = 0.48$	Calculated
Steel	Lagrangian	$\rho = 7{,}850\ kg/m^3$	
		$E = 207.0\ GPa$	
		$\nu = 0.3$	

Table 2: First Solution Attempt - Material Properties

Part	Type	Material Properties	Reference
Skull	Lagrangian	$\rho = 1{,}300\ kg/m^3$	(Baeck et al., 2011)
		$E = 15.0\ GPa$	
		$\nu = 0.22$	
Brain	Eulerian	$\rho = 1{,}060\ kg/m^3$	
		$K = 2.190\ GPa$	
		$G_o = 12.5\ kPa$	
		$G_\infty = 2.5\ kPa$	
		$\beta = 80\ s^{-1}$	
		$E = 35{,}193\ Pa$	Calculated
CSF	Lagrangian	$\rho = 1{,}000\ kg/m^3$	(Baeck et al., 2011)
		$E = 15.0\ MPa$	
		$K = 2.5\ GPa$	
		$\nu = 0.48$	Calculated

Table 3: Second and Third Solution Attempts - Material Properties

Furthermore, general contact properties were applied between all modeled parts. Pinned boundary conditions were applied to 45 nodes around the perimeter of the skull's base surface to prevent the skull from freely moving into space at impact. A constant velocity boundary condition was also applied to the impactor's geometry.

Although the simulation ran successfully, the results were not. It was observed that the velocity would not remain constant throughout the time step. In addition, the head acceleration and brain pressure computations produced abnormally high results. In an effort to correct the results produced by this model, it was decided to apply Nahum's load amplitude curve to the impactor, as opposed to a constant velocity. Therefore, the pertaining load amplitude curve was evenly distributed to the 231 nodes that make up the rear surface of the impactor.

The third solution attempt was also unsuccessful as the velocity would still not remain constant throughout the time step and the head acceleration and brain pressure plots revealed similarly high values as in the previous solution attempt.

At that point, it was decided to attempt a Lagrangian solution, as opposed to a coupled Eulerian-Lagrangian solution. The impactor's material properties were modified to reflect that of the impactor's covering layer, i.e., a foam pad. The corresponding geometry is shown in Fig. 5. This geometry closely resembles that in Fig. 4, with the exception of the brain geometry. As opposed to using a Eulerian-meshed brain, which encompasses the entire assembly, a Langrangian-meshed brain was used.

The boundary conditions were modified by applying pinned boundary conditions to 25 nodes at the centroid of the skull's base surface. This was done to simulate the actual neck motion constraint, since the cadaver in Nahum's experiment was positioned sitting down in a chair. Pinned boundary conditions were also applied to two nodes (four nodes in total) on each side of the skull at the ear level, since the ears in the experiment were constrained by sutures. The impactor was

given boundary conditions about its local axis (*x*-axis parallel with the length of the impactor). Specifically, it was constrained with respect to translation along the global *y*- and *z*-axis and with respect to rotation about all three axes. A constant, yet reduced, speed was also applied to the impactor. Since the impactor in the experiment was padded, the 9.94 m/s velocity value was reduced to 3 m/s. However, the computed solution displayed similar characteristics as in the previous solution attempts and, thus, was deemed unsuccessful.

In a subsequent effort to improve the results, it was decided to remove the impactor and apply Nahum's load amplitude curve directly to the skull, as opposed to utilizing an impactor with a constant velocity. Furhtermore, due to the short duration of the experiment, the head was given free boundary conditions as recommended in Horgan & Gilchrist (2003). The load amplitude curve was evenly distributed to the 35 nodes that make up the compact area between the skull and the impactor.

Unfortunately, this solution attempt also proved to be unsuccessful; the computed head acceleration and frontal pressure plots revealed a second oscillation towards the end of the simulation, which is inconsistent with Nahum's findings (Nahum et al., 1976). An additional solution attempt using modified brain material properties with values obtained from Ganpule (2013), and listed in Table 4, also proved unsuccessful.

Part	Type	Material Properties	Reference
Brain	Lagrangian	$\rho = 1{,}040$ kg/m^3	(Ganpule, 2013)
		$K = 2.19$ MPa	
		$G_o = 7.8$ kPa	
		$G_\infty = 41.0$ kPa	
		$\beta = 80$ s^{-1}	
		$E = 72{,}859$	
		$\nu = 0.49$	Calculated
		$\bar{g}_i^P = 0.8098$	
		$\bar{k}_i^P = 0.0$	
		$\tau_i = 0.0014$	

Table 4: Brain Material Properties – First Modification

. In an effort to improve the results, it was decided to modify the angle of the impactor force from 45 degrees to a 36.3-degree angle with respect to the horizontal plane as suggested in El Sayed et al. (2008). Neither this solution attempt though produced results close to the experimental ones.

Subsequently, it was decided to reset the Poisson's ratio value to 0.49 for both the brain and the CSF material, in addition to utilizing a combined set of material properties. The elastic modulus properties from (Baeck et al., 2011) were applied, combined with the viscoelastic properties recommended in (Ganpule, 2013). The pertaining values are listed in Table 5.

Part	Type	Material Properties	Reference
Brain	Lagrangian	$\rho = 1{,}060$ kg/m^3	(Baeck et al., 2011)
		$K = 2.19$ GPa	
		$G_o = 41.0$ kPa	(Ganpule, 2013)
		$G_\infty = 7.80$ kPa	
		$\beta = 700$ s^{-1}	
		$E = 16{,}536$ Pa	Calculated
		$\nu = 0.49$	Calculated
		$\bar{g}_i^P = 0.8098$	Calculated
		$\bar{k}_i^P = 0.0$	Calculated
		$\tau_i = 0.0014$	Calculated

Table 5: Brain Material Properties – Second Modification

In this case, the computed magnitude of the head acceleration as a function of time remained slightly larger than Nahum's results but within a reasonable range. Therefore, it was decided that the material properties listed in Table 5 should be utilized to validate the FEA model in Abaqus/CAE.

5.4 SOLUTION PROCESS

To summarize the successful solution attempt reported in Section 5.3, three sequential, explicit steps are followed. The first step is to apply boundary conditions to the model. For the

considered validation model, free constraints are utilized. The second step is to apply a load amplitude curve (see Appendix B) to the contact surface of the skull and to distribute it evenly between each of the 35 nodes that make up the contact area between the skull and the impactor, as displayed in Figure 7.

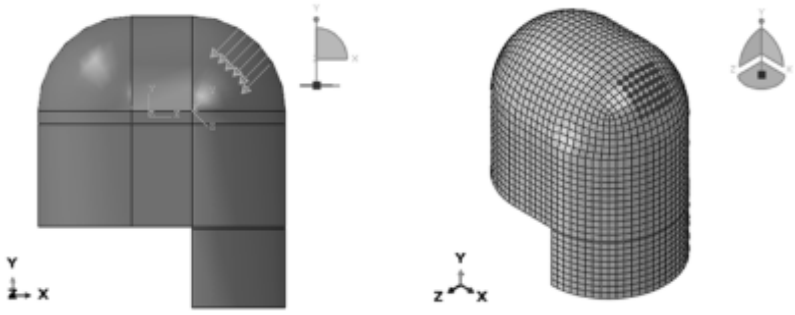

Figure 7: Validation Model Applied Load Curve

The time intervals and the corresponding force load curve applied to the validation model are measured and scaled using the data provided in (Nahum et al., 1977) pertaining to Experiment 37.

The third step is to define the interaction between the surfaces of the mating parts (described in detail in Section 4.3.2), which consists of tangential behavior and normal behavior. The tangential behavior utilizes the penalty formulation with an isotropic friction coefficient of 0.2. This value of the friction coefficient was successfully used in Song et al. (2015), and particularly at the interface between the skull and the impactor. It needs to be noted that this friction coefficient value is used for tangential contact between all contacting surfaces. The normal behavior has a "hard" contact pressure-overclosure relationship. This relationship minimizes penetration of the slave surface into the master surface at the constraint locations. Therefore, Abaqus/CAE separates the adjacent surfaces if the contact pressure reduces to zero. This is viewed

as the ideal relationship because it allows compressive stresses to transfer across the interface, but not tensile stresses, which is representative of the mating parts actual situation.

5.5 VALIDATION OF FEA MODEL RESULTS

The computed results from the validation model are graphed to produce a direct comparison to Nahum's sample data records for Experiment 37 (Nahum et al., 1977). The focus of this validation process is on the head acceleration. An additional criterion, the Head Injury Criterion (HIC), is also computed.

5.5.1 Head Acceleration

The head acceleration is calculated by Abaqus/CAE at node no. 17536 located in the vicinity of the solid model's center of gravity, as shown in Fig. 8. The maximum head acceleration calculated by Nahum for Experiment 37 is illustrated in Fig. 9 at 2,000 m/s^2 and compared to the

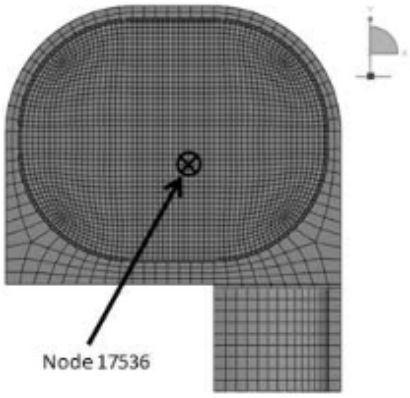

Figure 8: Solid Model Center of Gravity

validation model's acceleration.

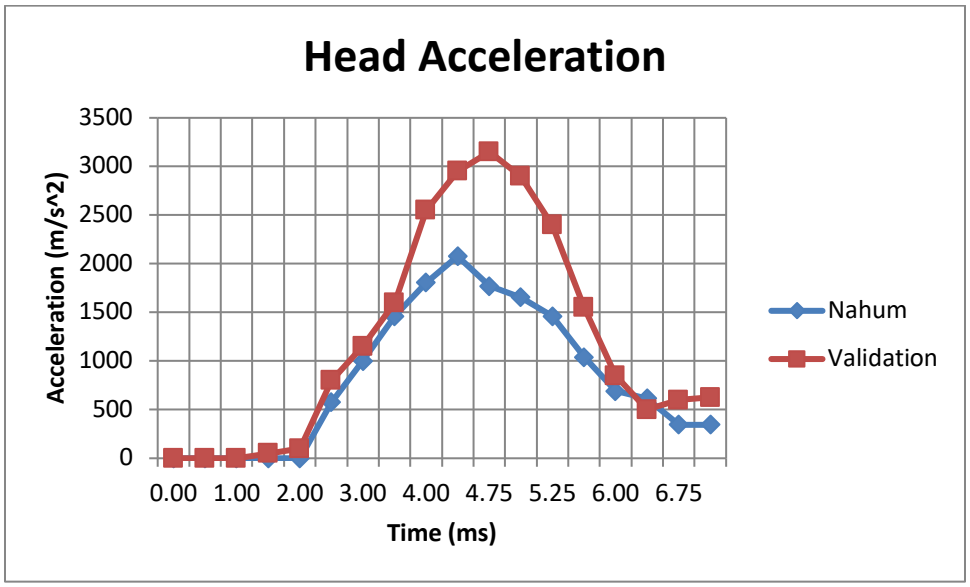

Figure 9: Head Acceleration vs. Time

As a method of interpreting the severity of the acceleration experienced by the human head during impact, the Head Injury Criterion (HIC) is calculated. The HIC is a method used extensively by the automotive industry to measure injury. The HIC for Nahum's data is confirmed by attempting to replicate the calculation as follows:

Vertex Form of a Vertical Parabola: $y = a(x - h)^2 + k$

Vertex of the Parabola: (h, k)

$$h = 0.0031 + \left(\frac{0.0055 - 0.0031}{2}\right) = 0.0043$$

$$k = 2{,}000$$

Equidistant Point from the Vertex: (x, y)

$$x = 0.0055$$

$$y = 1{,}000$$

Solve for Variable a: $1{,}000 = a(0.0055 - 0.0043)^2 + 2{,}000$

$$a = -6.94444x10^8$$

Acceleration, $a(t)$ in Vertex Form of a Parabola:

$$y(x) = (-6.94444x10^8)(x - 0.0043)^2 + 2{,}000$$

$$a(t) = (-6.94444x10^8)(t - 0.0043)^2 + 2{,}000$$

The average value $\bar{a}$ of the acceleration $a(t)$ over the time interval t_1 to t_2 is given by:

$$t_1 = 0.0031$$

$$t_2 = 0.0055$$

$$\bar{a} = \frac{1}{t_2 - t_1}\int_{t_1}^{t_2} a(t)dt$$

For the HIC, this is modified (based on experimental data) as follows:

$$HIC = max(t_1 \text{ or } t_2)\left\{(t_2 - t_1)\left[\frac{1}{t_2 - t_1}\int_{t_1}^{t_2} a(t)dt\right]^{2.5}\right\}$$

$$HIC = (t_2)\left\{(t_2 - t_1)\left[\frac{1}{t_2 - t_1}\int_{t_1}^{t_2} a(t)dt\right]^{2.5}\right\} = 1{,}496.91$$

The HIC is based on both the acceleration and deceleration; it is divided by two, due to symmetry:

$$HIC_{acc} = \frac{HIC}{2} = 748.455$$

$$HIC_{acc} = 749$$

The percent error compared to Nahum's calculated HIC value for Experiment 37 is:

$$HIC_{Nahum} = 744$$

$$\%_{error} = \left(\frac{|749 - 744|}{744}\right) \times 100\%$$

$$\%_{error} = 0.6\%$$

This percent error of the calculated HIC value to the documented value is considered negligible and validates that the mathematical formula used to calculate it is precise. To put this value into perspective, Table 1-2 in (Dehghani, 2012) per ASTM-F1292-04, is utilized to interpret

the results: Nahum's computed HIC value for Experiment 37 constitutes as a minor-to-moderate injury.

For the validation model, the computed HIC value is:

$$HIC_{validation} = 773$$

and the corresponding relative error:

$$\%_{error} = \left(\frac{|773 - 744|}{744}\right) \times 100\%$$

$$\%_{error} = 3.9\%$$

CHAPTER 6

MMA IMPACT MODEL

The sole purpose of creating and successfully solving the validation model is to ensure that an accurate FEA model is being utilized to analyze the effects of an MMA strike to the human head. With that model complete, it can be easily modified to simulate a head strike from an MMA practitioner. Prior to performing an FEA on the potential head trauma, data had to be collected to achieve not only an accurate result but a realistic one as well.

6.1 EXPERIMENTAL DATA

Due to the risk of injury in obtaining experimental data first hand, pre-existing data compiled on *National Geographic Channel's* television episodes titled, *Calculating the Ultimate Warrior* (National Geographic Society, Fight Science Calculating the Ultimate Warrior, 2007), *Mixed Martial Arts* (National Geographic Society, Fight Science Mixed Martial Arts, 2008), and *Stealth Fighters* (National Geographic Society, Fight Science Stealth Fighters, 2008) were used to complete this research. Portions of all three episodes were used to measure the force and damage of martial art's strikes using subject matter experts in various mixed martial arts disciplines.

For each episode, National Geographic assembled a fight science team of engineers and analysists to lead each experiment. The team on the episode titled *Calculating the Ultimate Warrior*, consisted of three members. The team leader was Randy Kelly, a mechanical engineer and Vice President of Denton ATD, Inc., a leading manufacturer of anthropomorphic test devices, commonly known as crash test dummies. The second team member was Dr. Tim Walilko, a biomedical engineer and senior scientist at Applied Research Associates, Inc. The third team member was James Lew, a member of the martial arts hall of fame, fight director and stunt coordinator. Mr. Lew's key role was the interpreter between the engineers and fighters.

The team on the episode titled, *Mixed Martial Arts*, consisted of three members as well. The first member and team leader was Dr. Cynthia Bir, a biomedical engineer and professor employed by Wayne State University. Supporting team members consisted of Randy Kelly of Denton ATD, Inc. and David Sandler of StrengthPro, Inc. Mr. Sandler is a sports physiologist and training expert for StrengthPro, Inc.

The equipment used for each experiment on the two episodes titled, *Calculating the Ultimate Warrior* and *Mixed Martial Arts* used to measure the force of each strike was a Hybrid III anthropomorphic test device (ATD) otherwise known as a crash test dummy. The specific model of the of the Hybrid III crash test dummy was not specified but it was stated that it was a typical model used in the automotive industry. Based on this information it was assumed to be a Hybrid III 50th percentile male ATD since it is the most widely used human impacting surrogate and has historically been used in automotive or military testing. The size and weight of the 50th Percentile Male Pedestrian Test Dummy represents an "average" of the USA adult male population (Hybrid III 50M Pedestrian | Humanetics ATD, 2018). This dummy design incorporates the ranges of motion, centers of gravity and body part weights defined by the Society of Automotive Engineers' anthropometric studies to simulate those of human subjects. This particular dummy was outfitted with sensors and measurement capabilities, allowing the fight science team to measure impact of blows, throws and kicks.

The team on the episode titled, Stealth Fighters, consisted of two members. The first member and team leader was Dr. Cynthia Bir, a biomedical engineer and professor employed by Wayne State University. The supporting team member was David Sandler of StrengthPro, Inc.

The equipment used for each experiment on the episode titled, Stealth Fighters is a heavy bag, outfitted with an accelerometer and a wireless accelerometer that was put around the ankle of

each fighter's ankle. Multiplying the mass of the object (i.e. heavy bag and fighter's leg) by the recorded acceleration will equate to the exact force generated by each strike.

Each test participant from the two episodes titled, *Calculating the Ultimate Warrior* and *Mixed Martial Arts* were given one opportunity to strike the secured Hybrid III ATD in the head with their fist. In addition, each test participant from the episode titled, *Stealth Fighters* was given one opportunity to strike the secured accelerometer equipped heavy bag with his style kick of choice. All participants are recognized as subject matter experts either in a specific fighting discipline or MMA in general. The episode titled *Calculating the Ultimate Warrior* tested the striking power of four specific MMA practitioners by the names of Alex Huynh, Mark Hicks, Bren Foster, and Steve Petramale. The episode titled *Mixed Martial Arts* tested two MMA fighters by the names of Randy Couture and Bas Rutten. The episode titled *Stealth Fighters* tested four marital artists by the names of Lateef Crowder, Simon Rhee, Levi Kurtovich, and Bren Foster. Alex Huynh is a three-time Kung Fu gold medalist in the Pan American Wushu Games. Mark Hicks is an expert in Karate. Bren Foster is a 5th level blackbelt in Tae Kwon Do and a former world champion. Steve Petramale is a fight trainer and undefeated professional boxer. Randy Couture is a master in ground fighting and a former MMA champion of the Ultimate Fighting Championship (UFC) who is best known for winning two titles in two weight classes. Since his time of fighting in the UFC, he has been inducted into the UFC Hall of Fame. Bas Rutten is a former undefeated UFC heavy weight champion, famed for his power striking. Lateef Crowder is a 25-year practitioner of Brazilian discipline martial art known as Capoeira. Simon Rhee is a 7th degree black belt of a traditional Japanese martial art known as Karate. Levi Kurtovich is a mixed martial arts fighter and practitioner of an Asian kickboxing art known as Muay Thai. The three strikers capable of producing the largest impactor force for their respective strike are listed in Table 6 with their method of striking to the head and the force generated from that strike.

Fighter	Strike	Impact (lbs)	Episode
Steve Petramale	Boxing Punch (Right Cross)	993	Calculating the Ultimate Warrior
Bas Rutten	Left Hook	1,291	Mixed Martial Arts
Bren Foster	Roundhouse Kick	2,300	Stealth Fighters

Table 6: Experimental Test Subjects

Steve Petramale produced a 993 lb boxing punch, known as a right cross. To successfully throw a cross, you must start with your base and transfer your energy from your feet up to your fist. Your fist should be tucked in front of your face with your elbows pointing down. Keep your knees bent, with the leg opposite of your striking fist leading and then pivot on your rear foot, like you are squishing a bug. Transfer your weight into your heel and at the same time, twist your hips while extending your rear hand outward straight out from chin level, while keeping your opposite hand up to guard. Just before your fist makes contact, turn it over so your knuckles are horizontal with the floor.

Bas Rutten produced a 1,291 lb left hook. To successfully throw a hook, you must start with your base and transfer your energy from your feet up to your fist, just as if you were throwing a cross. Keep your right arm up to guard your face and bring your left arm up, parallel to the ground. Bend your left arm 90 degrees as if you are holding shield and throw it into your target, making your fist contact their chin or temple.

Bren Foster produced a 2,300 lb right roundhouse kick. To successfully throw a roundhouse kick, you must start with contact being made with the ball of the foot. And the front foot planted. Raise the knee of your striking leg vertical, while pivoting the hips. Then snap the leg out to hit the target.

The brain, CSF and skull geometry used in the validation model are identical to that used the geometry used in the MMA impact model.

6.2 MMA IMPACT MODEL DETAILS

The primary difference between each MMA model is the surface area of the impactor (i.e. fist, leg, etc.). The surface area of Steve Petramale's right cross punch consisted of an estimated length and width of an average, man-sized fist. It was estimated as an 88.9 mm x 63.5 mm rectangle (0.005645 m^2) but modeled as a 79.5 mm x 66.3 mm (0.005271 m^2) due to the mesh size. The area of his fist, shown in Fig. 10, was aligned with the front location of the modeled skull, with the length, i.e. thumb to pinky, parallel to the global *z*-axis.

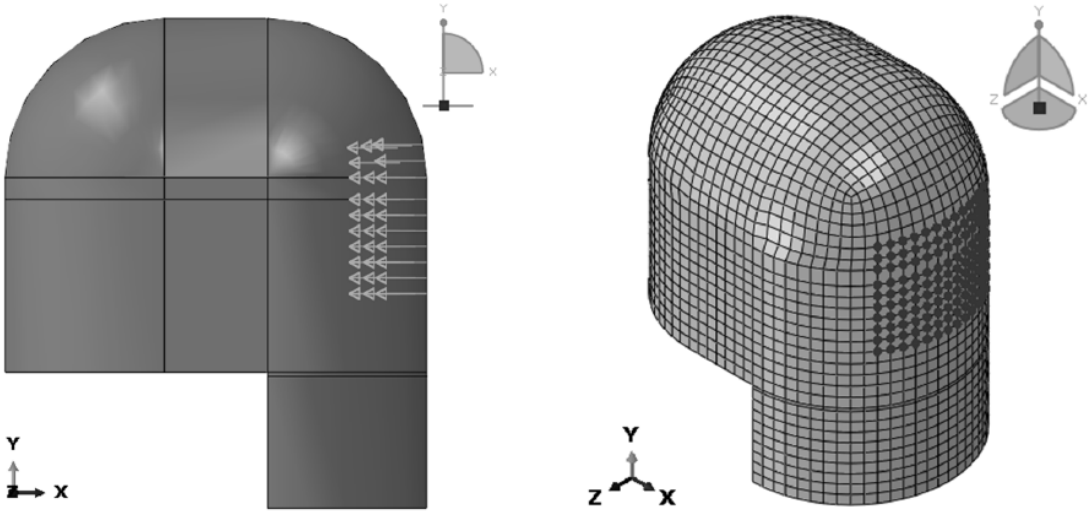

Figure 10: MMA Impact Model – Steve Petramale's Right Cross Punch

The surface area of Bas Rutten's left hook punch consisted of an estimated length and width of an average, man-sized fist. It was estimated as a 63.5 mm x 88.9 mm rectangle (0.005645 m^2) but modeled as a 62.6 mm x 84.1 mm (0.005265 m^2) due to the mesh size. The area of his fist, shown in Fig. 11, was aligned with the right temporal

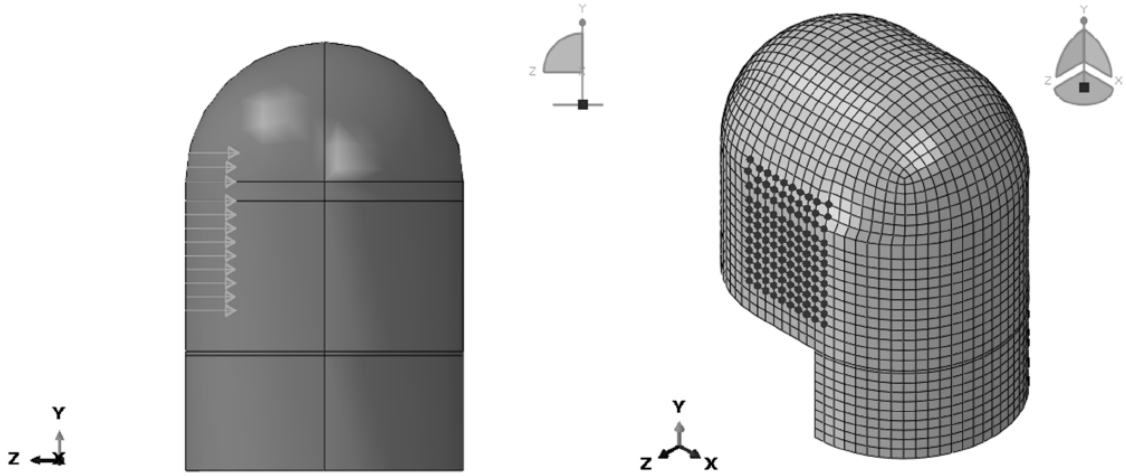

Figure 11: MMA Impact Model – Bas Rutten's Left Hook Punch

location of the modeled skull, with the length, i.e. thumb to pinky, parallel to the global *y*-axis.

The surface area of Bren Foster's right roundhouse kick consisted of an estimated length and width of an average, shin. It was estimated as a 50.8 mm x 76.2 mm rectangle (0.003871 m^2) but modeled as a 47.0 mm x 75.4 mm (0.003545 m^2) due to the mesh size. The area of his

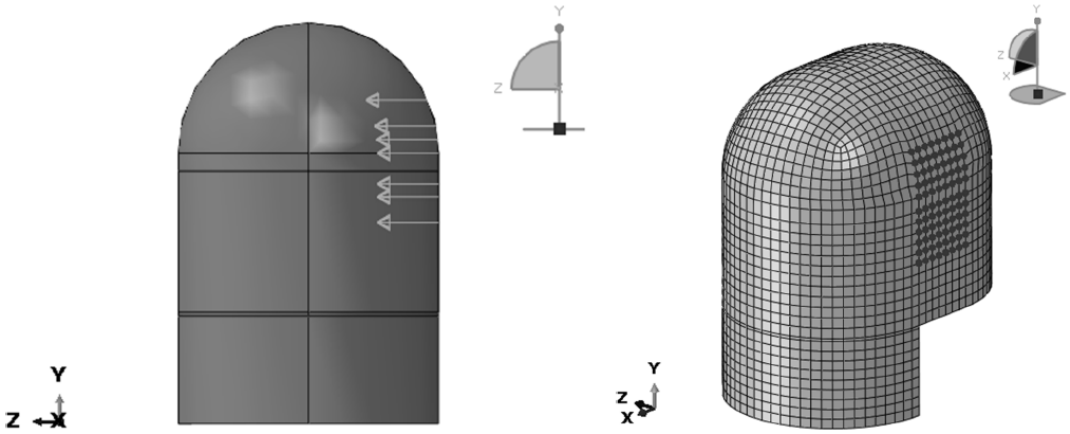

Figure 12: MMA Impact Model – Bren Foster's Right Roundhouse Kick

shin, shown in Fig. 12, was aligned with the left temporal location of the modeled skull, with the shin length parallel with the global *x*-axis.

The modeling details of the MMA impact model are almost identical to that of the validation model. The two key differences are the surface area of the impact as described in and the impact load amplitude (Appendices C through E). The surface area consists of the following number of nodes. Steve Petramale's right cross punch consists of 130 nodes, while Bas Rutten's left hook punch consists of 120 nodes, and Bren Foster's right roundhouse kick consists of 88 nodes. Similar to the validation model, the maximum load is divided evenly amongst each individual model's node set with the peak value being 20% of each individual's maximum resultant load, as displayed in Table 6. Although the peak load value is the primary focus of the load curve, it is important to note that this value is scaled in an identical fashion as the validation model's impact load amplitude (see Appendix B).

6.3 MMA IMPACT MODEL RESULTS

The data collected from the MMA models is graphed in order to understand the severity of the potential brain injury endured by MMA athletes. The following time dependent data is analyzed: head acceleration, HIC, and brain pressure on the impact side. The time dependent data is analyzed on a 7-ms time interval.

6.3.1 Head Acceleration

Just as the validation model, the head acceleration is computed by Abaqus/CAE at node no. 17536 located in the vicinity of the solid model's center of gravity (see Fig. 8). The maximum head acceleration calculated for the right cross punch, left hook punch, and right roundhouse kick are illustrated in Figs. 13 through 15. The 747 HIC score calculated for the right cross punch constitutes a minor injury endured by the fighter.

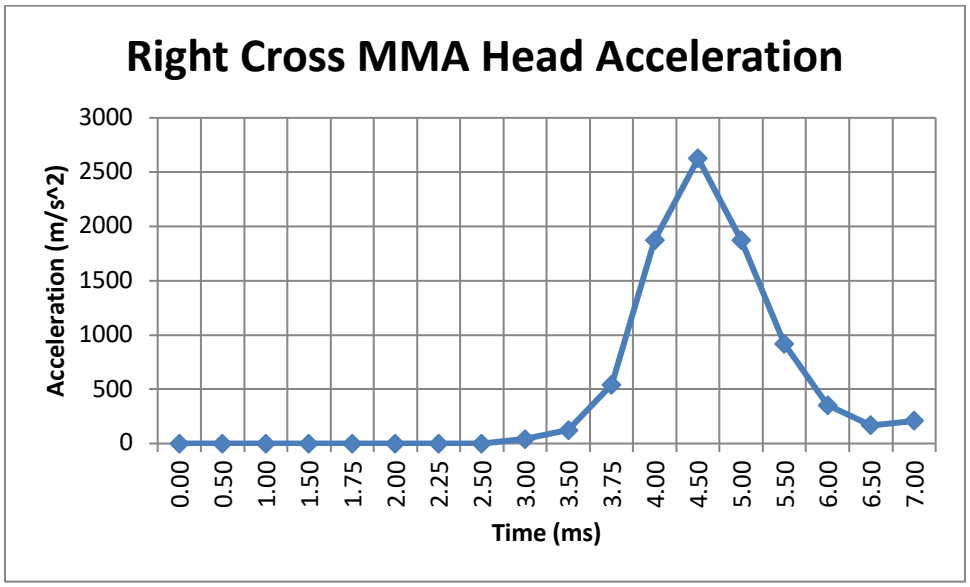

Figure 13: Head Acceleration vs. Time, Right Cross Punch

$$HIC_{cross} = 747$$

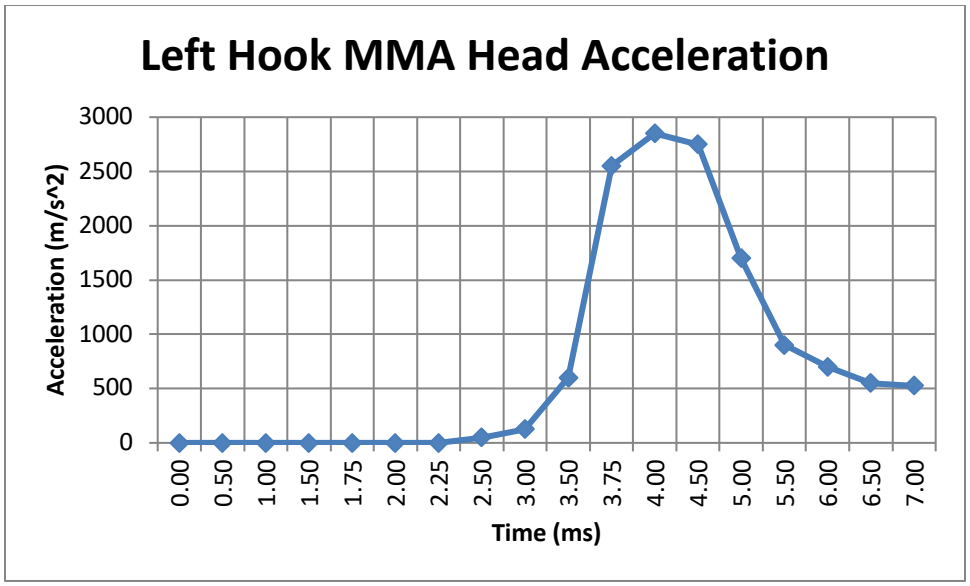

Figure 14: Head Acceleration vs. Time, Left Hook Punch

$$HIC_{hook} = 1{,}903$$

The 1,903 HIC score calculated for the left hook punch constitutes a moderate injury endured by the fighter.

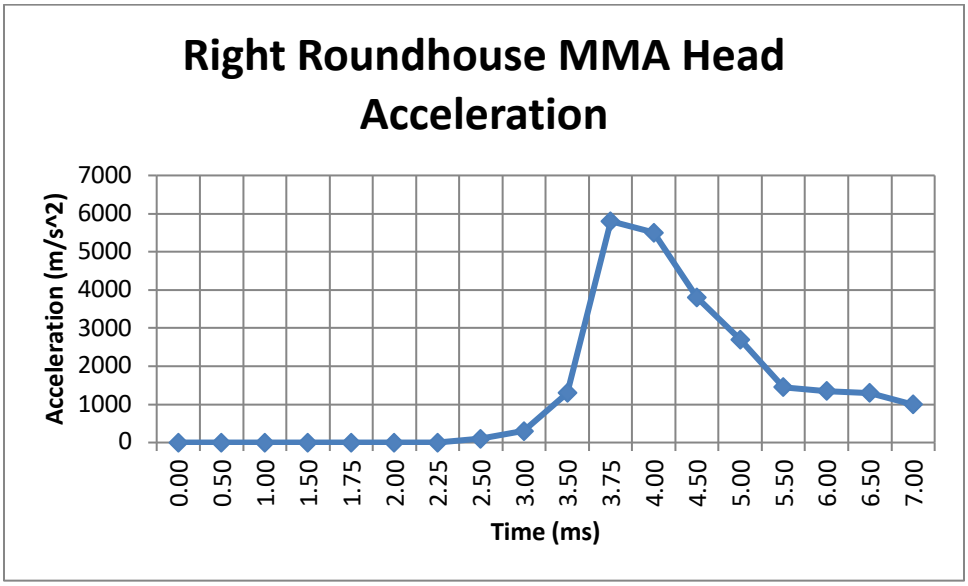

Figure 15: Head Acceleration vs. Time, Right Roundhouse Kick

$$HIC_{roundhouse} = 3{,}880$$

The 3,880 HIC score calculated for the right roundhouse kick constitutes a potentially fatal injury endured by the fighter.

6.3.2 Impact Side Pressure

The pressure due to impact for each strike is calculated by Abaqus/CAE at an element located normal to the impactor contact surface (see Figs. 16, 18, and 20). Per (Neurotrauma: Intracranial Pressure, 2007), the normal intracranial pressure (ICP) reading should be between 5 mmHg (667 Pa) to 15 mmHg (2,000 Pa). Patients experiencing ICP levels greater than 20 mmHg, (2,666 Pa) are typically treated for intracranial hypertension. As identified in this research, the brain pressure resulting from MMA strikes greatly exceeds this ICP threshold, meaning there is a high probability of brain injury.

The impact side pressure for the right cross punch was calculated by Abaqus/CAE at element no. 956 located normal to the fist's contact surface, as shown in Fig. 16.

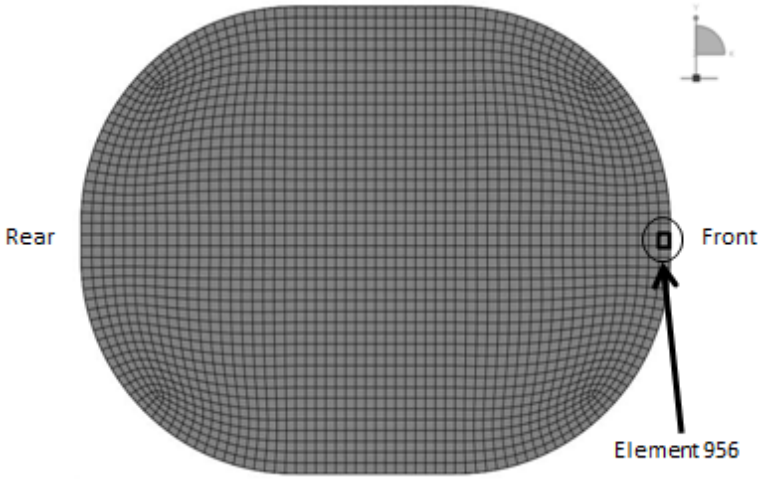

Figure 16: Location of Right Cross Punch Impact Side Pressure Reading

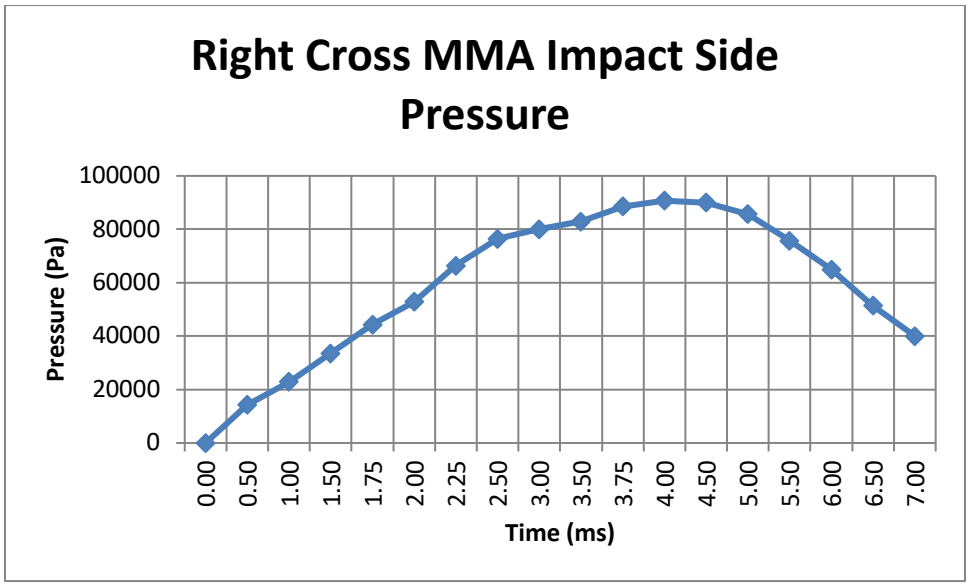

Figure 17: Impact Side Pressure vs. Time, Right Cross Punch

The impact side pressure for the left hook punch is calculated by Abaqus/CAE at element no. 65,082 located normal to the fist's contact surface, as shown in Fig. 19.

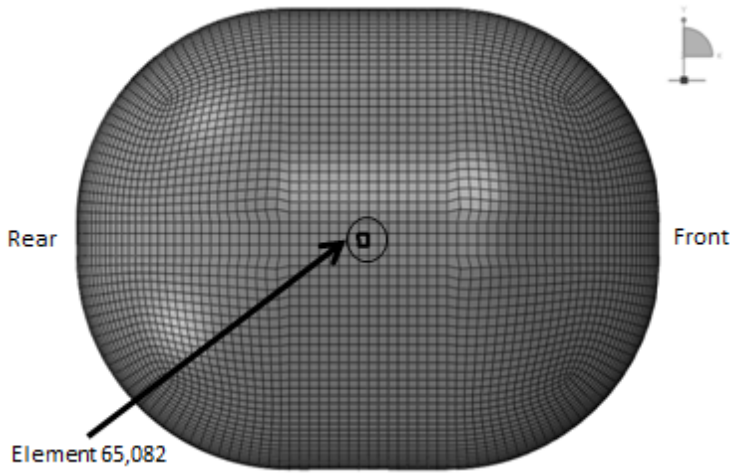

Figure 18: Location of Left Hook Punch Impact Side Pressure Reading

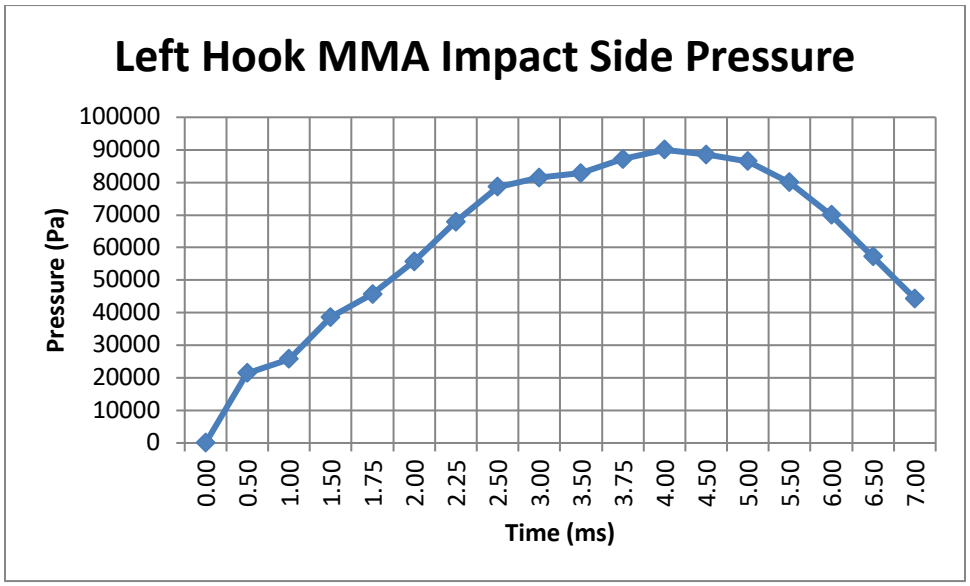

Figure 19: Impact Side Pressure vs. Time, Left Hook Punch

The impact side pressure for the right roundhouse kick is calculated by Abaqus/CAE at element no. 24,975 located normal to the leg's contact surface, as shown in Fig. 21.

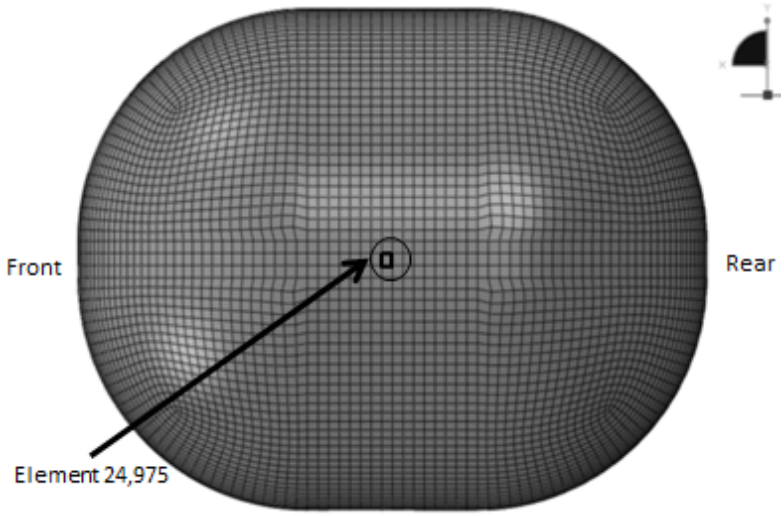

Figure 20: Location of Right Roundhouse Kick Impact Side Pressure Reading

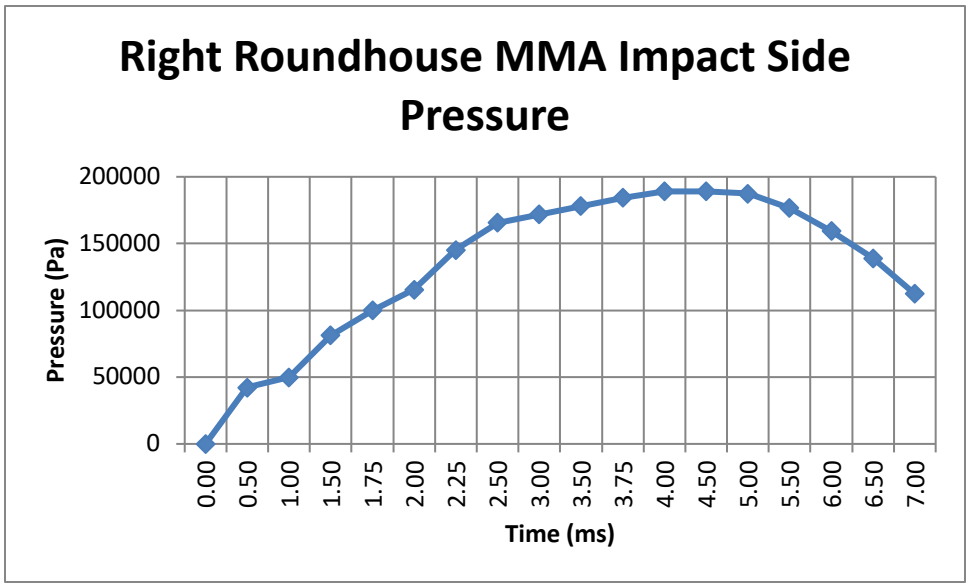

Figure 21: Impact Side Pressure vs. Time, Right Roundhouse Kick

CHAPTER 7

CONCLUSIONS AND FUTURE RESEARCH

The validation model is the predecessor to the MMA model, so if one model produces inaccurate results, then both models potentially do. As documented in Chapter 4, the validation model's computational results were not identical to those produced by Nahum. However, they were in a reasonable magnitude range. To understand how these results can be improved in future research, it is necessary to identify what assumptions were originally made and what could have been done to remedy incorrect or invalid results.

To start with, the CSF was modeled as an isotropic, elastic material, which means it has compressive properties. In reality, the CSF is nearly incompressible, and will experience no shear stress, i.e., $G = 0$. Baeck et al. (2011) go as far as proving the type of material used to represent the CSF (elastic vs. fluid) has no significant impact on the resulting stress. However, the strain energy in the CSF increases as a fluid, while reducing the strain energy applied to the brain. The same principle applies when it comes to increasing the number of elements that make up the thickness of the CSF. The number of elements that make up the elastic CSF does not make a significant change in the CSF and brain pressure, strain energy, and/or stress. It does however; make a difference when the material is represented as a fluid. The largest contributor to a change is stress and/or strain will be the material properties themselves.

Another factor is the bone material. The validation model supported by this research assigned constant material properties throughout the thickness of the bone. In reality, the bone is a composite material with the outer layers (compact) being more rigid and dense, while the center layer (diploë) is spongy in nature. This assumption may have added more weight to the skull, which could have played a factor on the head's acceleration. In addition, it may have caused the

skull to be more rigid then it actually is. This could have affected how well the skull absorbs the impactor.

The free constraint theory appeared to be the more reasonable assumption as it was proven to be more effective by multiple subject matter experts. Due to the short duration (i.e. 25 ms) of impact, applying free constraints made sense. By applying pinned or fixed restraints to the skull may have resulted in the brain absorbing an abnormal amount of pressure by oscillating much faster and harder than hypothesized. The same theory applies when it comes to the impactor as well. By applying constraints, the impactor may not bounce of the skull the way it should, or it may be forced to resist its natural trajectory.

When it comes to how the different materials interact with one another, you can choose to have a continuum scenario between each part or apply a friction factor. A continuum scenario will ensure that each part will have a more fluid interaction with one another. You risk not having that by simply applying some type of friction coefficient. Although, it may be the more accurate representation of the material, it has the potential to effect element distortion. For example, when that brain begins to oscillate, the CSF elements and/or the brain elements may just collapse on themselves opposed to rebounding with its mating material.

The simplification in the brain, CSF, and skull geometry played a significant role. By removing all the detail in the geometry (i.e. brain lobes, brain stem, hollow skull cavities), you risk not identifying the high stress concentration areas. Also, the frequency of the brain oscillation may increase with the simplified geometry. Not to mention misrepresenting of a part. For example, the brain stem was removed from the geometry. This modification alone will greatly affect the pressure readings in the posterior fossa. The tradeoff is achieving a higher quality mesh.

Another factor that can alter the data is the material properties used for the bone. A normal person (i.e. non-MMA athlete) will have a skull that is less dense in comparison to somebody who

practices high contact sports. As the bone endures repeated trauma, it tends to become denser. This is the theory behind a kickboxer spending years of his life repeatedly kicking hard objects during practice with his shin. It not only allows him to become acclimated to the pain, it also hardens the bone, reducing the risk of it breaking.

Last, but not least, there is the issue of the foam pad applied to the impactor. For the validation model used in this research, the impactor, nor the pad were utilized. A load applied to a premeasured area on the skull that equated to the desired force was incorporated instead. With this being the chosen method, it was discovered that using Nahum's load curve produced results of a much higher magnitude. To remedy this issue, the applied load curve had to be reduced by a predetermined factor to partially account for the foam pad.

REFERENCES

Abrahams, Dr. Peter. How the Body Works. London: Amber Books Ltd, 2007.

Baeck, K., J. Goffin and J. Vander Sloten. "The Use of Different CSF Representations in a Numerical Head Model and Their Effect on the Results of FE Head Impact Analyses." 8th European LS-DYNA Users Conference. Strasbourg, 2011.

Belingardi, Giovanni, Giorgio Chiandussi and Ivan Gaviglio. "Development and Validation of a New Finite Element Model of Human Head." n.d.

Carriere, R., & Moses, R. L. (1992). High Resolution Radar Target Modeling Using a Modified Prony Estimator. *IEEE Transactions on Antennas and Propagation*, 13-18.

Check Quality. 16 August 2012. 23 December 2017 <http://manual.midasuser.com/EN_Common/FEA/330/FEA/05_Mesh/Check_Quality.htm>.

Dehghani, H. (2012). *Optimal Impact Isolation for Minimal Head Injury Criterion (HIC) Using Effective Operating Region (EOR).* Burnaby: Simon Fraser University.

El Sayed, Tamer , et al. "Biomechanics of Traumatic Brain Injury." Comput. Methods Appl. Mech. Engrg. (2008): 4692-4701.

Ganpule, Shailesh Govind. Mechanics of Blast Loading on Post-Mortem Human and Surrogate Heads in the Study of Traumatic Brain Injury (TBI) Using Experimental and Computational Approaches. Ph.D. Dissertation. University of Nebraska. Lincoln, 2013.

Getting Started with Abaqus: Interactive Edition (6.14). 23 April 2014. 27 December 2017 <http://127.0.0.1:2080/v6.14/books/gsa/default.htm?startat=book01.html#gsa>.

Gleiber, M. A. (2018, April 20). *Four Common Injuries in MMA and UFC Fighters*. Retrieved from Michael Gleiber Md, MD, PA Concierge Spine Surgery: https://www.michaelgleibermd.com/news/4-common-injuries-mma-ufc-fighters/

Hashemi, Javad and William Fortune Smith. Foundations of Materials Science and Engineering. New York: The McGraw-Hill, 2006.

Horgan, T J and M D Gilchrist. "The Creation of Three-Dimensional Finite Element Models for Simulating Head Impact Biomechanics." IJCrash 8.4 (2003): 353-366.

Hybrid III 50M Pedestrian | Humanetics ATD. 27 January 2018. 27 January 2018 <http://www.humaneticsatd.com/crash-test-dummies/pedestrian/hybrid-iii-50m>.

Jacob, Paul and Lee Goulding. An Explicit Finite Element Primer. NAFEMS Ltd, 2002.

Kang, Ho-Sung, et al. "Validation of a 3D Anatomic Human Head Model and Replication of Head Impact in Motorcycle Accident by Finite Element Modeling." SAE Technical Paper 973339 (1997): 329-338.

Lazo, Denise L. Fundamentals of Sectional Anatomy: An Imaging Approach. Stamford: Cengage Learning, 2015.

MMA Uniform Rules. (2018, November 24). Retrieved from Epic Sports: https://mma.epicsports.com/mma-uniform-rules.html

Nahum, Alan M., Carley C. Ward and Randall W. Smith. "Intracranial Pressure Dynamics During Head Impact." SAE Technical Paper 770922 (1977): 338-366.

Nahum, Alan M. and Randall W. Smith. "An Experimental Model for Closed Head Impact Injury." SAE Technical Paper 760825 (1976): 2638-2651.

National Geographic Society. Fight Science Calculating the Ultimate Warrior. 30 April 2007.

National Geographic Society. Fight Science Mixed Martial Arts. 27 January 2008.

National Geographic Society. Stealth Fighters. 1 May 2008.

Neurotrauma: Intracranial Pressure. (2007, February 3). Retrieved from Trauma.org:

http://www.trauma.org/archive/neuro/icp.html

The Finite Element Method - Theory. 1 December 2017. December 2017 <http://illustrations.marin.ntnu.no/structures/analysis/FEM/theory/index.html>.

Unified Rules of Mixed Martial Arts. (2018, November 24). Retrieved from UFC: https://www.ufc.com/unified-rules-mixed-martial-arts

Willinger, Remy, Ho-Sung Kang and Baye Diaw. "Three-Dimensional Human Head Finite-Element Model Validation Against Two Experimental Impacts." Annals of Biomedical Engineering (1999): 403-410.

Xuewei Song, Cong Wang, Hao Hu, Tianlun Huang, and Jingxu Jin "A Finite Element Study of the Dynamic Response of Brain Based on Two Parasagittal Slice Models." Computational and Mathematical Methods in Medicine (2015): 1-14.

APPENDIX A

PRONY METHOD MATLAB CODE

PronyC.m

```
function[c,ceq,Deq] = PronyC(x);

        function [out1,out2,outn] = function_name (in1, in2, inn)
                function [max_val,max_loc] = my_max(v)
global NPC;

c = sum(x(1:NPC))-1;
ceq = [];
Deq = [];

end
```

PronyF.m

```
function f = PronyF(x)
global NTSP NPC NDV tpi gn;
gp = ones(NTSP,1) - sum((ones(NTSP,1)*x(1,1:NPC)).*(ones(NTSP,NPC)-exp(-
(tpi'*ones(1,NPC))./(ones(NTSP,1)*x(1,NPC+1:NDV)))),2);
f = (sum((gp-gn').^2,1));
end
```

PronyOpt.m

```
clear,clc,clearvars, close all
global NDV NPC NTSP tpi gn lbs ubs;
format long;
NPC = 2;
NDV = 2*NPC;
rt_upper = 1;
NTSP = 250;
G0 = 41000;
G00 = 7800;
beta = 700;
tpi = linspace(0,(NTSP-1)/1000,NTSP);
G = zeros(NTSP,1);
G = G00 + (G0-G00)*exp(-beta*tpi);
gn = G./G0;
lbs = zeros(1,NDV);
ubs = ones(1,NDV);
x0 = rt_upper*rand(1,NDV);
options = optimoptions('fmincon','Display','iter','Algorithm','sqp');
[prony,fval,exitflag,output] = fmincon(@PronyF,x0,[],[],[],[],lbs,ubs,@PronyC,options);
gp = ones(NTSP,1) - sum((ones(NTSP,1)*prony(1:NPC)).*(ones(NTSP,NPC)-exp(-
(tpi'*ones(1,NPC))./(ones(NTSP,1)*prony(NPC+1:NDV)))),2);
error = (sum((gp(:,1)-gn').^2,1))/NTSP;
hold on;
plot(tpi,G0*gn)
plot(tpi,G0*gp')
hold off;
```

APPENDIX B

VALIDATION MODEL: IMPACTOR SCALED INPUT FORCE DATA

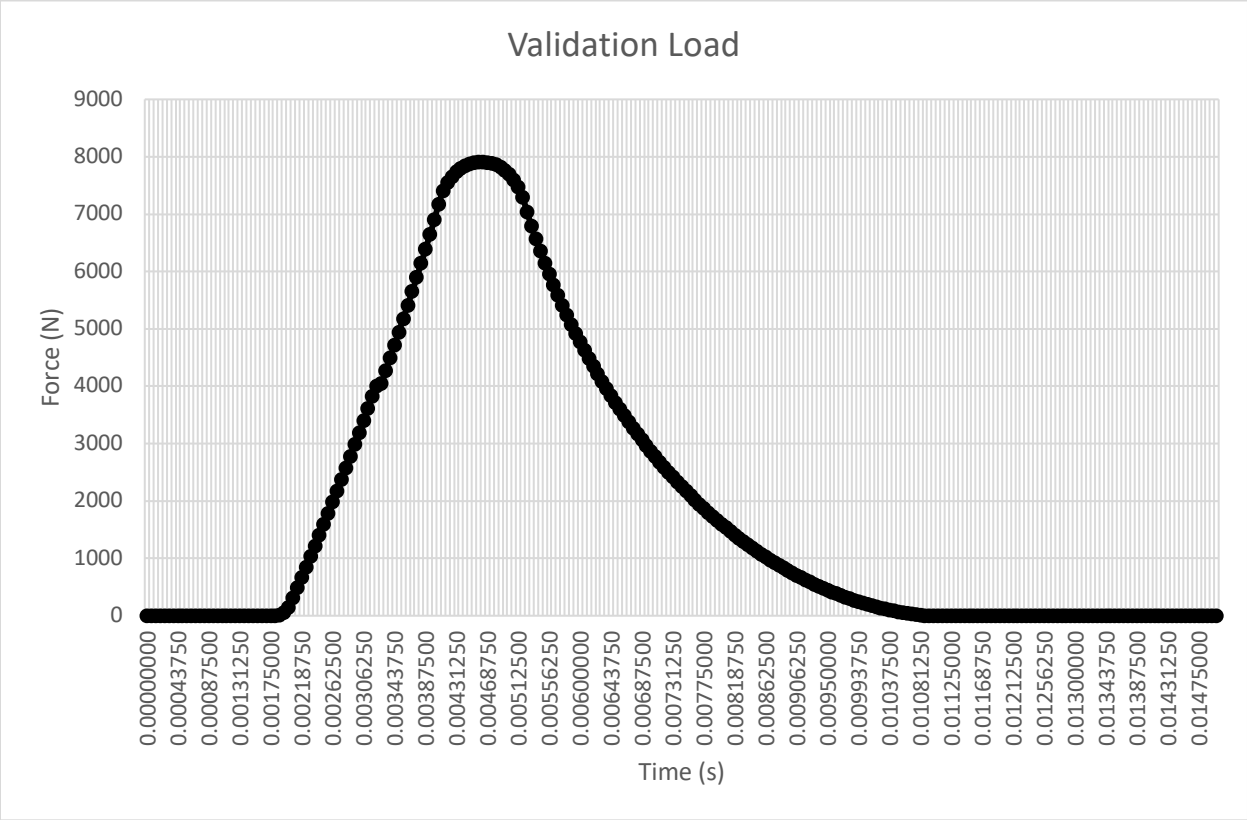

APPENDIX C

MMA MODEL: RIGHT CROSS PUNCH SCALED FORCE DATA

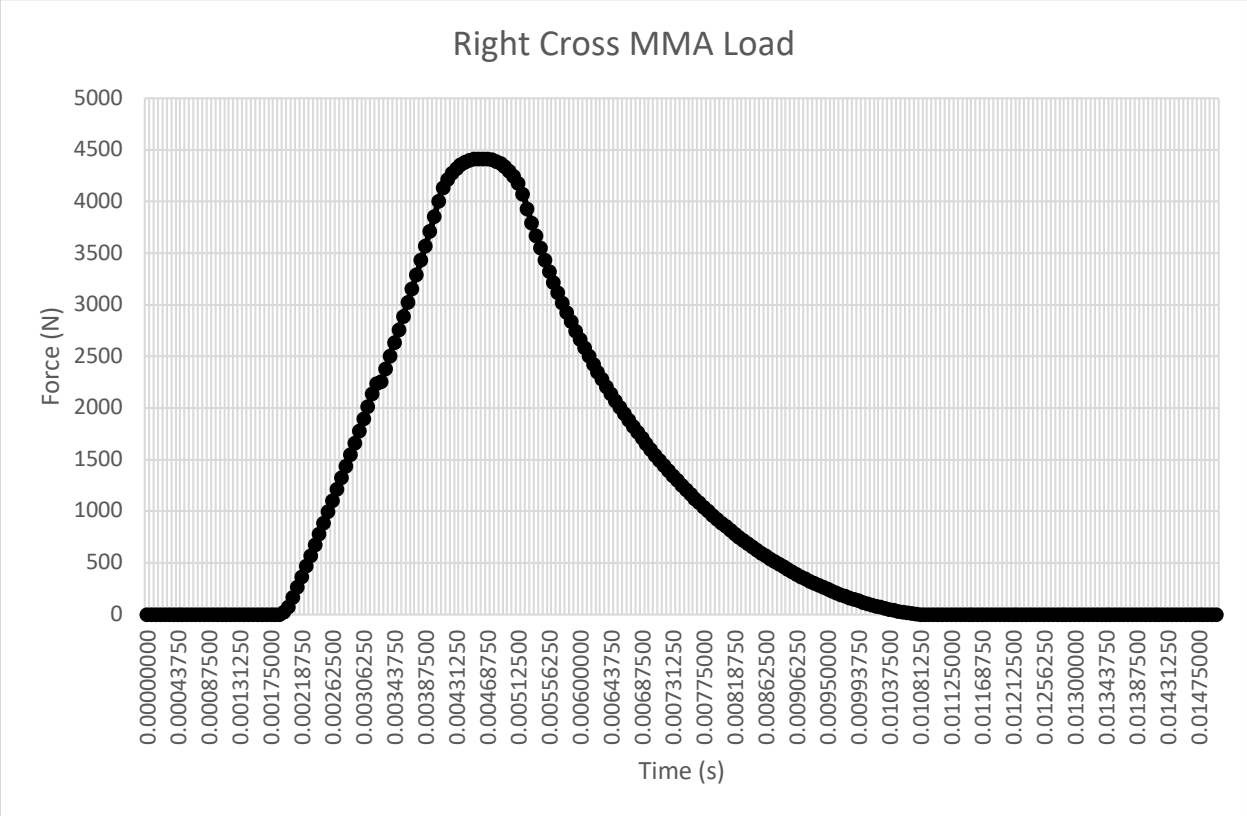

APPENDIX D

MMA MODEL: LEFT HOOK PUNCH SCALED FORCE DATA

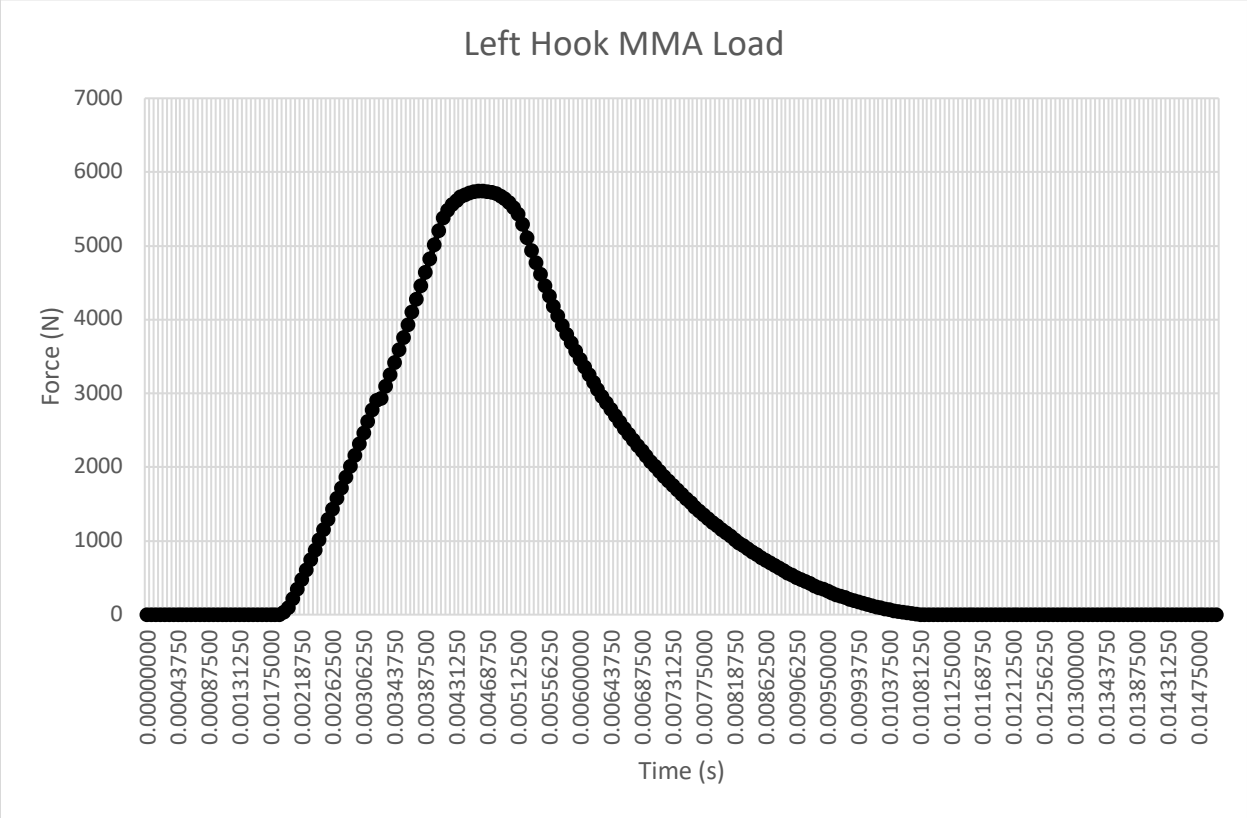

APPENDIX E

MMA MODEL: RIGHT ROUNDHOUSE KICK SCALED FORCE DATA

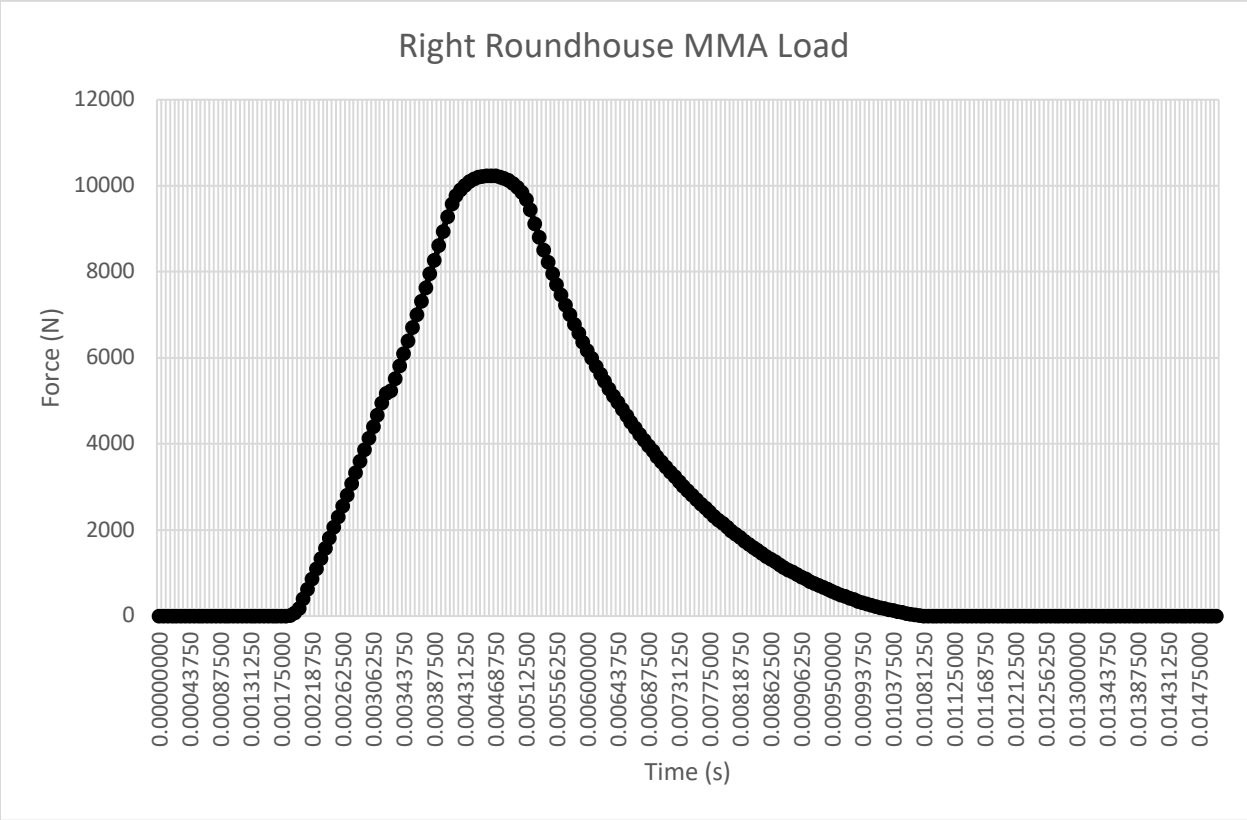

VITA

JOHN W.M. SORBELLO

Education

Master of Engineering in Mechanical Engineering at Old Dominion University, December 2018. Thesis Ttitle: “A Scientific Approach to Understanding the Head Trauma Endured by a Mixed Martial Arts Fighter.”

Bachelor of Science in Mechanical Engineering at Old Dominion University, December 2007.

Associate in Science in General Studies at Northern Virginia Community College, May 2003.

Career Certificate in Computer Aided Drafting at Northern Virginia Community College, May 2003.